Double resonance infrared–visible photofragment yield spectroscopy of NO_2: Interferences among overlapping quasibound levels

S. A. Reid and H. Reisler
Department of Chemistry, University of Southern California, Los Angeles, California 90089-0482

(Received 23 March 1994; accepted 24 June 1994)

We examine fluctuations in the unimolecular decomposition of state-selected NO_2 using double resonance infrared (IR)–visible and visible–IR photofragment yield (PHOFRY) spectroscopy. Spectra for specific NO(v,J,Λ,Ω) states at excess energies ($E^\dagger$)=2000–2525 cm^{-1} exhibit marked differences in the shapes, positions, and widths of the resonance structures. We interpret this effect as arising from interferences among coherently excited overlapping quasibound levels. Comparisons of IR–visible PHOFRY spectra with one-photon spectra in the same energy region and IR–visible spectra at lower $E^\dagger$ are used to assess the importance of thermal averaging (i.e., incoherent excitations) and to examine the transition from mild to more severe level overlap. The experimental results are compared qualitatively with results from sample calculations to shed further light on the interplay between dynamics and statistics in the decomposition and the role of overlapping quasibound levels.

I. INTRODUCTION

The success of statistical theories [e.g., the Rice–Ramsperger–Kassel–Marcus (RRKM) theory,[1] phase space theory (PST),[2] the statistical adiabatic channel model (SACM),[3] and their variants] in modeling experimental data for many unimolecular reactions has led to detailed studies of the manifestations of statistical behavior in small molecules. By investigating limiting cases where the assumptions of these theories [e.g., the independence hypothesis, complete vibrational energy redistribution (IVR) on the time scale of reaction] may not be valid, it is possible to examine the underlying causes of statistical behavior. Experimentally, the combination of monochromatic (laser) excitation and cold molecular beams can minimize both eigenstate and thermal averaging. These techniques were used, for example, in detailed studies of the barrierless unimolecular decompositions of NCNO (Refs. 4 and 5) and ketene,[6,7] which, despite their small size, are nevertheless well described by statistical theories.

Following much important (and sometimes conflicting) work over the past two decades,[3,8–16] recent experimental and theoretical results[17–25] have unambiguously shown that the barrierless unimolecular decomposition of NO_2 can be described within the framework of statistical theories. For example, rotational and vibrational state distributions of the NO($^2\Pi_\Omega;\Omega=1/2,3/2$) fragment formed in the decomposition of monoenergetic NO_2 samples at excess energies ($E^\dagger$) of 0–3038 cm^{-1} are well described on average by statistical theories (e.g., PST, variational RRKM theory);[11,17,20,21] however, significant fluctuations and oscillations are observed about the statistical predictions in each case. The unimolecular reaction rates at the same $E^\dagger$ also agree with statistical predictions.[9,19] The success of statistical theories in modeling NO_2 decomposition *on average* is perhaps not surprising; optical excitation prepares highly mixed states of primarily $^2B_2/^2A_1$ electronic character.[26–44] Vibronic chaos is already well established in NO_2 at energies >16 000 cm^{-1},[44] yet the small vibronic state density [$\rho_{ev}<1/cm^{-1}$, Refs. 10(a),10(b),15(a),15(b),44], near dissociation threshold [$D_0=25\,130\pm2$ cm^{-1}, Refs. 10(a),10(b),24(b),45] suggests that deviations from statistical behavior might also be expected.

In previous work on NO_2,[17,18] we examined fluctuations in both NO product state distributions (PSD's) and state-specific photofragment yield (PHOFRY) spectra. The PHOFRY spectra of specific NO($^2\Pi_\Omega,v,J,\Lambda$) states, where Λ is the lambda-doublet component, exhibited marked differences in the shapes, positions, and widths of resonance structures, yet some strong correlations were observed. In particular, NO($v=0$) levels of similar J generally exhibited well correlated PHOFRY spectra, a result reflected in NO($v=0$) rotational state distributions at the same $E^\dagger$, which typically exhibited oscillatory structures with widths of several J's. Well correlated spectra were also observed for $^2\Pi_{1/2}(J)$,$^2\Pi_{3/2}(J-1)$ [i.e., same N] pairs of levels; similarly, rotational state distributions in the two NO spin–orbit states exhibited excellent reproducibility. In contrast, a weak correlation was observed for PHOFRY spectra of levels in different vibrational manifolds, a result reflected in the different fluctuation patterns observed in NO $v=0$ and $v=1$ rotational state distributions at a specific $E^\dagger$. These results suggest that a hierarchy of adiabaticity exists in the evolution of the NO degrees of freedom along the reaction coordinate; vibrational excitation first becoming adiabatic followed by rotational and, at long range, electronic (i.e., spin–orbit) degrees of freedom.[18] To explain the fluctuations and oscillatory structures observed in both NO PSD's and one-photon PHOFRY spectra, we used a model that incorporated interferences among both overlapping quasibound states in the excited molecule and in the evolution of vibrational levels of the transition state (TS) into fragment degrees of freedom.[18]

Several studies have investigated the nature of the TS in NO_2 decomposition. Frequency domain experiments near dissociation threshold suggest that at threshold the TS is loose (i.e., PST-like).[21] This conclusion is supported by previous work on NCNO (Refs. 4,5) and ketene,[6,7] where the measured decomposition rates are described by PST near

threshold, but deviate from PST at $E^{\dagger}>170$ and 70 cm^{-1}, respectively.[4–7] The deviation from PST arises from a tightening of the TS with increasing energy; the location of the TS moves from atop long range orbital angular momentum barriers at low excess energies to smaller internuclear separations at higher energies.[5(b),7,20,25,47] The TS levels thus evolve from free-rotor states to anharmonic hindered rotor states to more harmonic bending-type levels. For NO_2, the TS tightens rather quickly; real-time measurements of $k(E)$ show pronounced steps, the first of which occurs at $E^{\dagger}\sim100$ cm^{-1}.[19] At higher energies, the TS levels are probably best described as low frequency (e.g., $\omega\sim100$ cm^{-1}) bending-type levels.[19,20,25]

From the rate measurements above D_0 and the parent density of states determined from high resolution spectra below D_0,[10(a),10(b),15(a),15(b),44,47] we conclude that NO_2 decomposition is characterized by overlapping quasibound states. Throughout this paper we refer to the lifetime-broadened $^2B_2/^2A_1$ states as quasibound states; spectral structures resulting from overlap and interferences among these levels are denoted resonances. One-photon excitation coherently and, at our rotational temperatures, also *incoherently* excites several to many overlapping $^2B_2/^2A_1$ quasibound states. This superposition is assumed to project randomly onto the energetically accessible vibrational levels of the TS; in turn, we assume that each bending like TS level maps onto a specific set of product quantum states. Projection through multiple TS levels and rapid passage from TS to products may lead to interferences. In this model, the marked dependence of the positions, shapes and widths of resonance structures on the monitored NO final state in one-photon PHOFRY spectra is attributed to different weightings of overlapped states; yet the strong correlations observed for specific $NO(v,J,\Lambda,\Omega)$ levels suggests they arise from similar weightings of TS levels, in turn arising from a similar superposition of excited quasibound states.

In this paper, we examine in detail the fluctuations and oscillatory structures previously observed in one-photon experiments. In particular, we identify *sources* of these fluctuations and assess their relevance to statistical theories. To assess the importance of thermal averaging (i.e., incoherent excitations), we employ double-resonance IR–visible and visible–IR excitation for parent state selection. Differences in selection rules preclude the direct comparison of one-photon and IR–visible (or visible–IR) PHOFRY spectra; we therefore use correlations *within* each set of spectra as a basis for comparison. As an additional aid in understanding the fluctuations and oscillations, we compare qualitatively some of our experimental results with sample calculations.

Fluctuations (or oscillations) in fragment rotational state distributions have been observed in direct dissociation from a well-characterized initial state. In a pioneering experiment, Andresen and co-workers observed a marked preference for levels of (−) total parity in the OH fragment from dissociation of H_2O following excitation to the repulsive $^1B_1$ surface from a single rovibrational level in the electronic ground state.[48] These oscillations are reproduced theoretically in Franck–Condon expansion of the ground state wave function onto the asymptotic set of OH quantum states.[49] Such a calculation is not realistic for NO_2, yet we note that fluctuations on the basis of parity might be expected; for jet-cooled NO_2 parity selection is inherent, as only rotational levels of even N are populated in the $K=0$ stack. We have not previously observed a population bias on the basis of total parity in the NO fragment at $E^{\dagger}>400$ cm^{-1},[17,18] yet note that above the threshold for production of excited $O(^3P_j;j=2,1,0)$ spin–orbit levels, conservation of total parity does not bias levels in the NO fragment. Welge and co-workers[10(a),10(b)] have observed parity oscillations for $J_{NO}<2.5$ at energies where only $O(^3P_2)$ is accessible; these oscillations disappear at higher J. Miyawaki *et al.*[21] examined the same energy region, but did not find a population bias on the basis of total parity. In any case, when all oxygen spin–orbit states are energetically accessible, parity oscillations in the NO PSD's are not expected.

Fluctuations arising from interferences among overlapping resonances are commonly observed in nuclear physics, and are known as "Ericson fluctuations."[50–55] Ericson's formalism goes beyond a statistical treatment which applies the random phase approximation, but still assumes that formation and decay of the complex are independent.[50] The phases of the overlapped levels are assumed to be uncorrelated (i.e., random), and the fluctuations are not damped but become more random as more levels overlap. Blümel and Smilansky have shown that Ericson fluctuations are expected in simple quantum mechanical systems whose classical analogs display irregular (i.e., chaotic) scattering.[55] To make the connection with transition state theories of unimolecular reaction, the Ericson-type fluctuations will be associated with a "loose" TS; here the direct scattering of overlapped levels in the excited molecule into final states is an appropriate description. Such is the case for NO_2 decomposition close to threshold. In this region the NO product state distributions exhibit fluctuation patterns which vary quite randomly from channel to channel, and are significantly damped when summing the distributions for the two Λ-doublet states.[10(a),10(b),17,21] These fluctuations are quite different from those observed at higher $E^{\dagger}$, where large oscillatory structures, which are well reproduced in the separate Λ-doublet state distributions, become prominent.[17,22,23] It is the goal of this work to more completely understand this phenomenon through detailed double-resonance experiments and sample calculations.

The outline of the paper is as follows. Section II describes the experimental techniques and methodologies. Section III presents our experimental results, consisting of IR–visible fluorescence excitation spectra, IR–visible and visible–IR PHOFRY spectra, and NO state distributions obtained with two-photon excitation. Section IV A begins the discussion, addressing changes in the reactive density of states above D_0 and implications for PHOFRY spectra. In Sec. IV B we describe a model that can account for all of our experimental results and illustrate it qualitatively with sample calculations. Section IV C describes the implications of our experimental results for the dissociation mechanism and compares results from one- and two-photon experiments.

II. EXPERIMENTAL METHOD

NO_2 samples (Matheson, 99.5%) are purified by repeated freeze–pump–thaw cycles in a dry ice/acetone bath. An equal 1%–5% mixture of purified NO_2/O_2 in He at total pressures of 600–1100 Torr is expanded into an octagonal vacuum chamber (base pressure$\sim 10^{-6}$ Torr), using a piezoelectrically actuated pulsed nozzle (0.5 mm diam orifice, 180 μs pulse width). The free jet is crossed ~15 mm downstream of the orifice at a 90° angle by three laser beams which are spatially overlapped and temporally delayed. Tunable infrared radiation (4–7 mJ/pulse, ~1 cm^{-1} bandwidth, 2×3 mm beam) is generated by a $LiNbO_3$ parametric oscillator (OPO) constructed in-house. Photolysis (in IR–visible experiments) or excitation (in visible–IR experiments) wavelengths are generated from an excimer pumped dye laser system (DPS/dioxane, coumarin 440/methanol, coumarin 450/methanol); typical pulse energies are 2–5 mJ in a 5 mm diam beam. Probe radiation at λ=220–230 nm is generated by frequency doubling the fundamental of a second excimer pumped dye laser system (coumarin 450/methanol) in a BBO crystal. Nascent $NO(^2\Pi_\Omega, v, J)$ fragments are detected by laser induced fluorescence (LIF) at a typical photolysis-probe delay of 200 ns; a similar delay is employed between excitation and photolysis pulses. Fluorescence is imaged by an f/0.67 objective lens onto the plane of a field stop. The magnified image at the field stop (×2.25) is collimated by a two lens telescope and projected through a "solar blind" filter onto the surface of a photomultiplier tube (PMT, Hamamatsu RU166H) oriented at 90° to both the axis of the jet and of the laser beams. The PMT signal is digitized by a digital storage oscilloscope and recorded by a computer, which controls data acquisition and laser frequency stepping.

Four types of experiments were carried out. First, an IR–visible fluorescence excitation spectrum of NO_2 was obtained by tuning the OPO frequency to excite the $R(2)$ transition in the $NO_2(101)$ band at 2908 cm^{-1}.[56–59] The excitation laser frequency was then scanned below dissociation threshold, and the resulting fluorescence monitored by a GaAs PMT. To avoid background fluorescence induced by the excitation laser alone, an interference filter [λ_{max}=420 nm, $\Delta\lambda$=25 nm (FWHM)] was used to view "resonance" fluorescence near the sum of the two excitation frequencies.

IR–visible PHOFRY spectra were obtained by tuning the OPO frequency to the same transition, tuning the probe laser frequency to excite a specific NO rovibrational transition in one spin–orbit manifold, and scanning the photolysis laser frequency to obtain a yield spectrum for dissociation into the monitored state. In a third arrangement, the excitation order was reversed; the tunable dye laser system was tuned to excite mixed $^2B_2/^2A_1$ rovibronic eigenstates ~2500 cm^{-1} below dissociation threshold, the probe laser frequency tuned to a specific NO rovibrational transition and the OPO frequency then scanned to obtain visible–IR PHOFRY spectra. In both arrangements probe pulse energies of 10–40 μJ (~5 mm beam diam) were used, and the OPO fired only on alternate shots to allow direct shot-to-shot subtraction of background NO signal arising from 2-photon 1-color dissociation by the photolysis (excitation) laser.[60] This background signal was virtually eliminated in our experimental configuration, and in all cases was more than one order of magnitude smaller than the 2-photon 2-color signal. PHOFRY spectra were smoothed using a Blackman window low-pass filter; smoothing improved S/N without altering the peak shapes.

In a fourth arrangement, NO rotational state distributions were obtained by tuning the OPO to the $R(2)$ line of the NO(101) band, tuning the excitation laser frequency to a specific $E^\dagger$, and scanning the probe laser frequency across the (0,0) band of the γ-system to map the NO $v=0$ rotational state distribution. Here probe pulse energies <3 μJ were used to avoid partial saturation of the NO transitions; peak intensities in all branches were converted to populations in the manner previously described.[17]

III. RESULTS

A. Selection rules for one- versus two-photon excitation: One-photon and IR–visible fluorescence excitation spectra below D_0

Considering the conserved representations of total spin–rovibronic symmetry (A_1 or A_2) and J, selection rules for one-photon excitation via the $^2B_2$ state are $A_1 \leftrightarrow A_2$ and $\Delta J=0,\pm 1$.[43,44] For jet-cooled NO_2 (T_{rot}<5 K) only levels of N=0, 2, and 4 ($J=N\pm 1/2$) of the K=0 (symmetric top notation) stack are significantly populated; these levels are of A_1 total spin–rovibronic symmetry. One-photon excitation from the ground state thus prepares eigenstates of A_2 symmetry and J=1/2–11/2. For IR–visible excitation via the $NO_2(101)$ state, selection rules in the infrared transition are $A_1 \leftrightarrow A_2$ and $\Delta J=0,\pm 1$;[58] infrared excitation on the $R(2)$ transition of the $\nu_1+\nu_3$ band populates levels of A_2 symmetry and J=5/2, 7/2. Subsequent electronic excitation prepares levels of A_1 symmetry and J=3/2–9/2; states of different symmetry are thus populated via two- vs one-photon excitation, with the total number of accessed levels reduced by more than a factor of 2. Note that visible–IR excitation also accesses levels of A_1 symmetry.

To illustrate differences in one- vs two-photon excitation, displayed in Fig. 1 are one-photon and IR–visible fluorescence excitation spectra taken at energies 0–120 cm^{-1} below dissociation threshold. As expected, the IR–visible spectrum is much less congested; in fact, many peaks in this spectrum appear significantly *narrower*. This reflects the higher degree of congestion in the one-photon spectrum, since the same excitation laser was used for both scans. The IR–visible spectrum more clearly reveals the sparse level density.[10(a),10(b),15(a),15(b),44] We note that relative absorption intensities of features in the IR–visible spectrum may not be accurately reflected, since only fluorescence at the sum of the excitation frequencies is viewed; however, all allowed transitions should be evidenced. Dispersed fluorescence spectra at lower energies clearly reveal a breakdown of vibronic symmetry selection rules in fluorescence.[44]

B. Photofragment yield (PHOFRY) spectroscopy

1. IR–visible PHOFRY spectroscopy

We have previously reported a detailed study of fluctuations in one-photon PHOFRY spectra at $E^\dagger$<2800 cm^{-1}.[18] These spectra exhibit prominent peaks of 4–100 cm^{-1} width

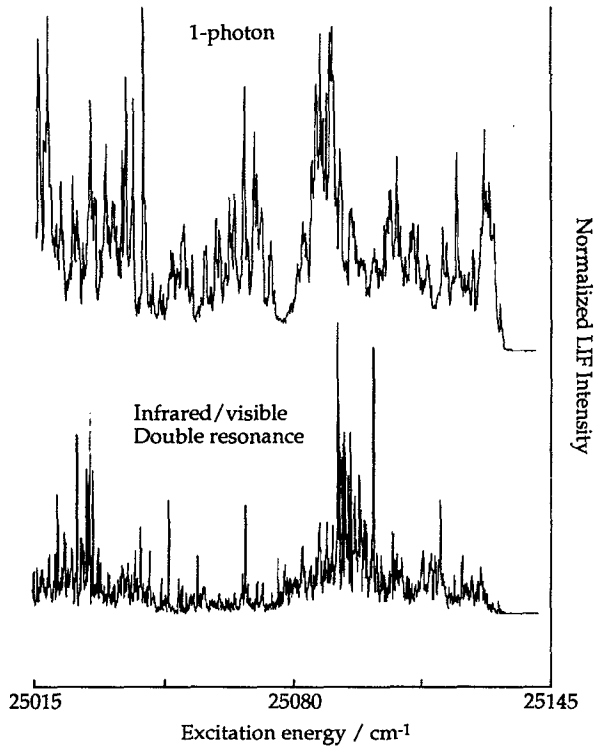

FIG. 1. One-photon and double-resonance IR–visible fluorescence excitation spectra of NO_2 in the region 0–120 cm^{-1} below dissociation threshold, obtained as described in the text.

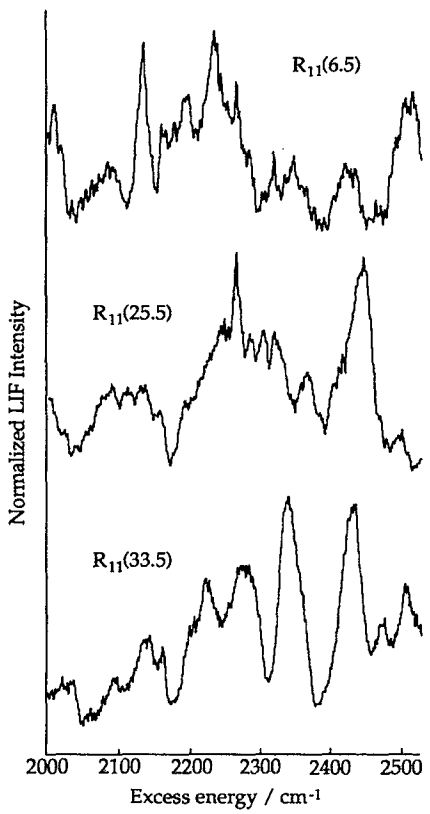

FIG. 2. IR–visible photofragment yield (PHOFRY) spectra of NO_2 at $E^{\dagger}$=2000–2525 cm^{-1} obtained by monitoring the R_{11} (6.5), R_{11} (25.5), and R_{11} (33.5) transitions of the (0,0) band of the NO γ-system.

(FWHM), and pronounced differences in the widths, positions, and shapes of resonance structures are observed when monitoring different NO(v,J) levels. Despite the differences, some clear correlations are also observed. In this work, we examine these correlations and the effects of thermal averaging with double resonance IR–visible and visible–IR PHOFRY spectroscopy.

A strong correlation is observed in one-photon PHOFRY spectra at $E^{\dagger}<2800$ cm^{-1} for NO ($v=0$) levels of similar total angular momentum, and a similar correlation was also observed at $E^{\dagger}=475-650$ cm^{-1} in double resonance IR–visible PHOFRY spectra.[18(a)] Displayed in Fig. 2 are three IR–visible PHOFRY spectra obtained at $E^{\dagger}=2000-2525$ cm^{-1} by monitoring NO($v=0$) levels over the range $J=6.5-33.5$. These spectra, which are highly structured, illustrate the pronounced differences in positions, widths and shapes of resonance structures observed when monitoring NO(v)

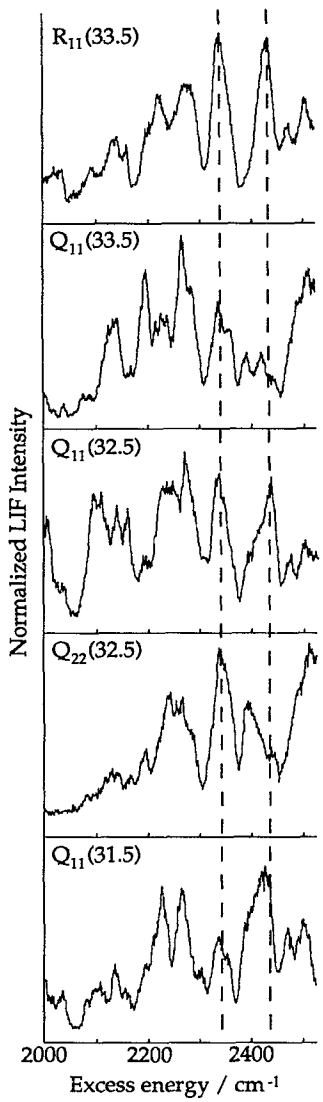

FIG. 3. IR–visible PHOFRY spectra of NO_2 at $E^{\dagger}=2000-2525$ cm^{-1} obtained by monitoring the R_{11} (33.5), Q_{11} (33.5), Q_{11} (32.5), Q_{22} (32.5), and Q_{11} (31.5) transitions of the NO(0,0) band.

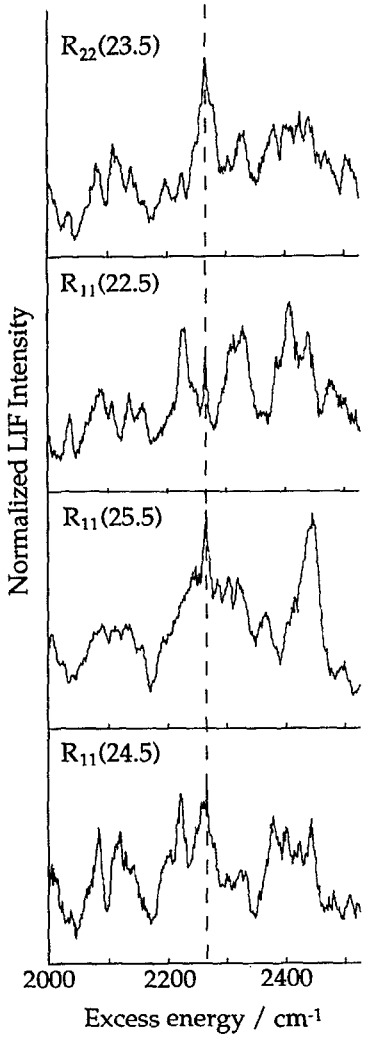

FIG. 4. IR–visible PHOFRY spectra of NO_2 at $E^{\dagger}$=2000–2525 cm^{-1} obtained by monitoring the R_{22} (23.5), R_{11} (22.5), R_{11} (25.5), and R_{11} (24.5) transitions of the NO(0,0) band.

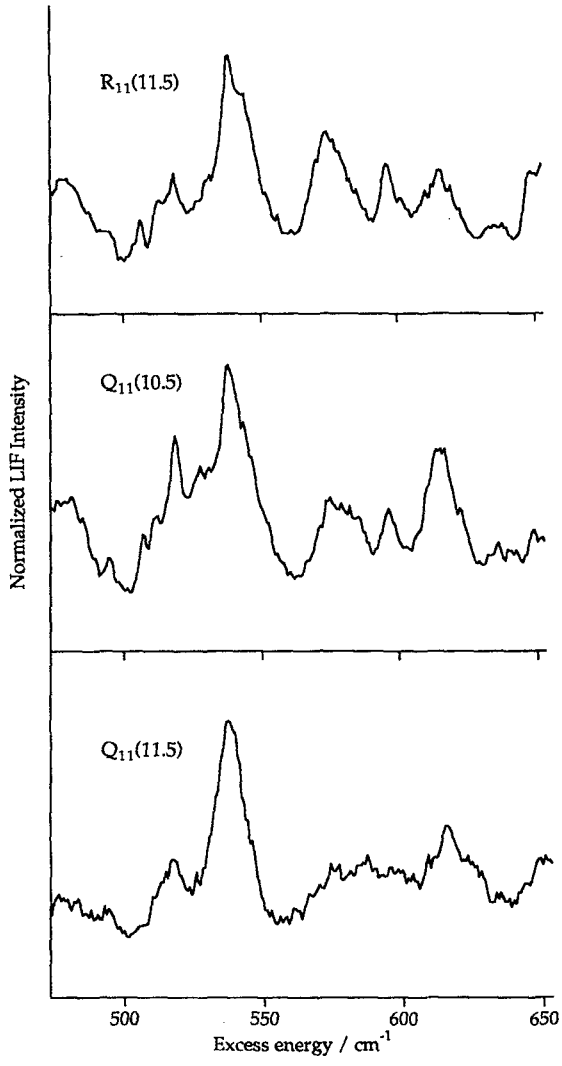

FIG. 5. IR–visible PHOFRY spectra at $E^{\dagger}$=475–650 cm^{-1} obtained by monitoring the Q_{11} (11.5), Q_{11} (10.5), and R_{11} (11.5) transitions of the NO(0,0) band.

levels of different J. This effect is observed in one-photon PHOFRY spectra in the same energy region;[18(b)] however, unlike the one-photon spectra, very different IR–visible PHOFRY spectra are obtained for levels of *similar* J as well. To illustrate, Fig. 3 displays five IR–visible PHOFRY spectra in the same energy region obtained for NO(v=0) levels of J=31.5–33.5. Globally, these spectra exhibit very different resonance structures, yet some similarities are observed; for example, two asymmetric features in the R_{11} (33.5) spectrum at $E^{\dagger}$~2340 and 2430 cm^{-1} (marked by dashed lines) are reproduced in the Q_{11} (32.5) spectrum. An intense peak at $E^{\dagger}$~2280 cm^{-1} is found in all five spectra, yet the shape of this peak varies significantly. Each spectrum also exhibits a central clump of peaks at $E^{\dagger}$~2180–2300 cm^{-1}, yet the structures within the clump change dramatically and no consistent correlations are observed. As a further illustration, Fig. 4 displays four IR–visible PHOFRY spectra of NO(v=0) levels in the range J=22.5–24.5. Each spectrum is highly structured, yet again the resonance structures exhibit little correlation. A central peak at $E^{\dagger}$~2266 cm^{-1} (marked by a dashed line) is seen in all four spectra, yet the width and shape of this peak changes significantly. In the R_{11}(22.5) spectrum this feature is of width ~3 cm^{-1} (FWHM), much narrower than the expected lifetime broadened width of ~15–20 cm^{-1} in this energy region.[3(g),9,19(a),19(b)]

We have previously reported a correlation based on J in IR–visible PHOFRY spectra taken at $E^{\dagger}$=475–650 cm^{-1};[18(a)] specifically, a stronger correlation was observed for spectra of NO(v=0) levels differing by 1 in J (i.e., J=11.5 vs J=10.5) than those for levels more widely separated in J (i.e., J=11.5 vs J=6.5) [see Fig. 3 of Ref. 18(a)]. To further illustrate this correlation, Fig. 5 displays three IR–visible PHOFRY spectra at $E^{\dagger}$=475–650 cm^{-1} for NO(v=0) levels of similar J; resonance structures in these spectra are obviously well correlated. To quantify this correlation, we use the measure of correlation that we have previously developed, i.e., the root-mean-square value of the

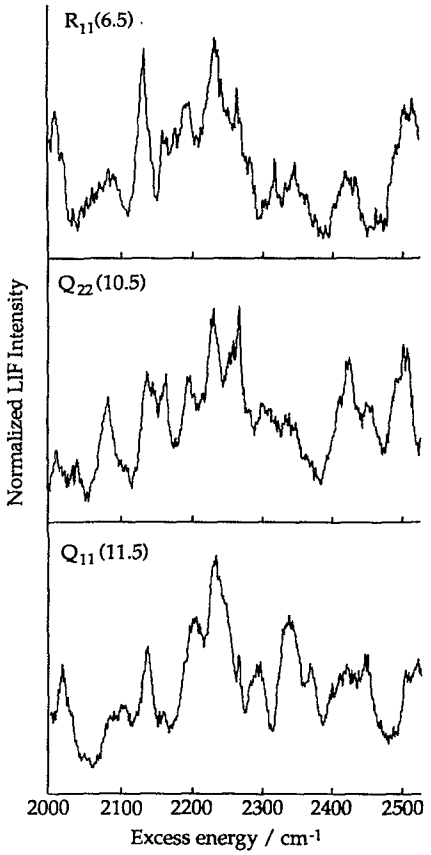

FIG. 6. IR–visible PHOFRY spectra of NO_2 at $E^{\dagger}=2000-2525$ cm^{-1} obtained by monitoring the R_{11} (6.5), Q_{22} (10.5), and Q_{11} (11.5) transitions of the NO(0,0) band.

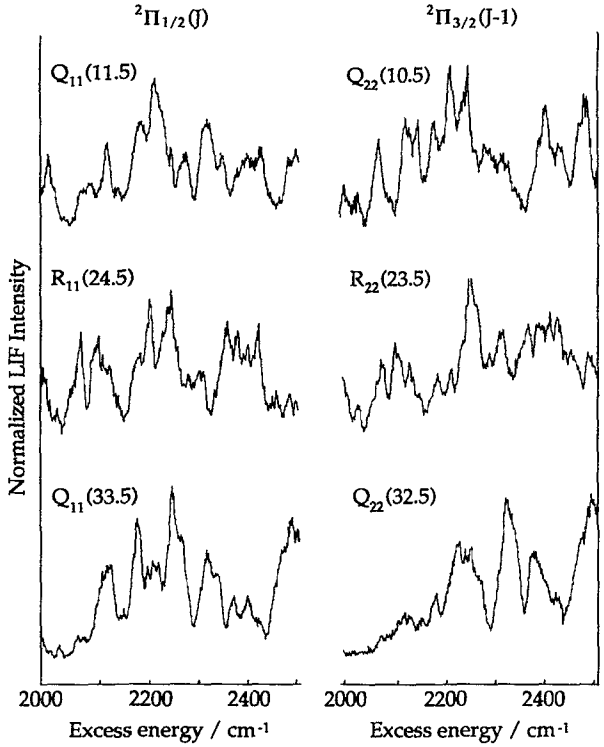

FIG. 7. IR–visible PHOFRY spectra of NO_2 at $E^{\dagger}=2000-2525$ cm^{-1} obtained for pairs of $^2\Pi_{1/2}(J)$, $^2\Pi_{1/2}(J-1)$ levels. These spectra were obtained by monitoring the Q_{11} (11.5) and Q_{22} (10.5), the R_{11} (24.5) and R_{22} (23.5), and the Q_{11} (33.5) and Q_{22} (32.5) transitions of the NO(0,0) band.

correlation index (CI_{rms}).[18(b)] The average CI_{rms} obtained from comparing pairs of these three spectra is 0.011, which is close to the lowest CI_{rms} of 0.009 (and thus the best correlation) previously observed in one-photon PHOFRY spectra.[18(b)] In contrast, a poorer correlation is found for spectra of levels differing by 5 or more in J, as evidenced by a CI_{rms} averaged over five pairs of spectra of 0.051. It is clear both visually and quantitatively that a correlation based on angular momentum exists here, yet a much poorer correlation is observed at higher $E^{\dagger}$. To illustrate, shown in Fig. 6 are three IR–visible PHOFRY spectra at $E^{\dagger}=2000-2525$ cm^{-1} obtained for NO($v=0$) levels of $J=6.5$, 10.5, and 11.5. Like those shown in Figs. 3 and 4, these spectra exhibit marked differences in resonance structures and no clear correlations are apparent. This is reflected in CI_{rms} values of 0.033 ($\Delta J=1$) and 0.031 ($\Delta J=5$). We have determined CI_{rms} for 12 pairs of IR–visible PHOFRY spectra at $E^{\dagger}=2000-2525$ cm^{-1} differing in J by 0 or 1, and 12 pairs differing in J by more than 5. The values fluctuate considerably with no obvious trends; average CI_{rms} are 0.041 ($\Delta J=0,1$) and 0.067 ($\Delta J>5$), which are much higher than the value of ~0.01 that we have previously defined as good correlation.[18(b)]

A second correlation evidenced in one-photon PHOFRY spectra is that for $^2\Pi_{1/2}(J)$,$^2\Pi_{3/2}(J-1)$ (i.e., same N) pairs of levels,[18(b)] a result reflected in the similarity of rotational state distributions in the two NO spin–orbit states at a given excess energy.[17] Displayed in Fig. 7 are three pairs of IR–visible PHOFRY spectra at $E^{\dagger}=2000-2525$ cm^{-1} comparing $^2\Pi_{1/2}(J)$,$^2\Pi_{3/2}(J-1)$ pairs of levels over a range of J. The spectra for levels within a given spin–orbit manifold (and thus of different J's) show marked differences in resonance structures as expected. However, while some similarities are observed, the $^2\Pi_{1/2}(J)$,$^2\Pi_{3/2}(J-1)$ pairs of spectra also display little correlation of resonance structures. We note that the average CI_{rms} for these three pairs of spectra (0.030) is slightly smaller than the average for all *other* pairs of spectra of similar J (0.044), however, this difference is well within the spread in the latter measurements (−0.21, +0.35).

A third correlation (or more precisely, lack thereof) observed in one-photon PHOFRY spectra is that for NO(v,J) levels in different *vibrational* manifolds, i.e., $v=0$ vs $v=1$. Specifically, a weak correlation of the $v=0$ and $v=1$ PHOFRY spectra on the basis of either total angular momentum or total rovibrational energy is evidenced. Displayed in Fig. 8 are three IR–visible PHOFRY spectra which probe NO levels in both $v=0$ and $v=1$. The upper two panels display spectra for identical levels in $v=0$ vs $v=1$, while the upper and lower panels exhibit spectra for $v=1$ vs $v=0$ levels at the same NO rovibrational energy. Marked differences in resonance structures are observed, particularly when comparing the $R_{11}(33.5)$ spectrum (lower panel) with either of

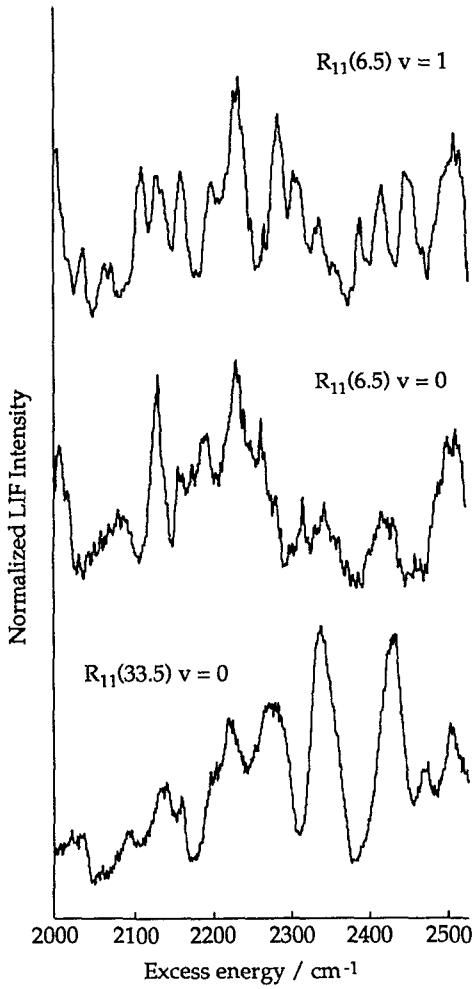

FIG. 8. IR–visible PHOFRY spectra of NO_2 at $E^{\dagger}$=2000–2525 cm^{-1} obtained by monitoring the R_{11} (6.5) transition of the NO(1,1) band and the R_{11} (6.5) and R_{11} (33.5) transitions of the NO(0,0) band.

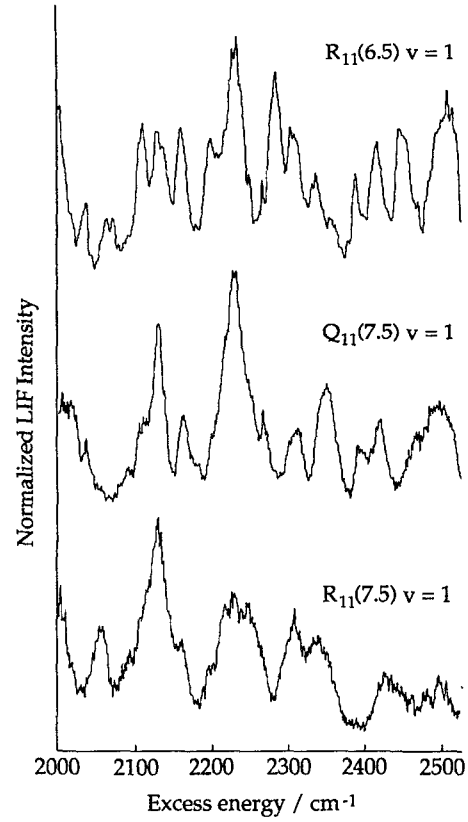

FIG. 9. IR–visible PHOFRY spectra of NO_2 at $E^{\dagger}$=2000–2525 cm^{-1} obtained by monitoring the R_{11} (6.5), Q_{11} (7.5), and R_{11} (7.5) transitions of the NO(1,1) band.

the other spectra. To compare, displayed in Fig. 9 are three spectra obtained by monitoring NO(v=1) levels of *similar J* (i.e., J=6.5 vs J=7.5). Like those NO(v=0) spectra shown in Figs. 3, 4, and 6, significantly different resonance structures are observed, as reflected in an average CI_{rms} of 0.033.

Finally, we discuss the *widths* of resonance structures in our IR–visible PHOFRY spectra. In the regime of overlapping levels, care must be used in comparing lifetimes determined from resonance structure widths to those predicted by statistical theories, e.g., the RRKM theory. Several recent theoretical studies based on random matrix theory[61–64] have investigated the distribution of resonance widths expected in the regime of strong overlap. Calculations predict extensive fluctuations about the mean width; in some cases, the distribution of widths *broadens* as the degree of overlap increases.[62] Mathematically, narrow resonances represent entrapment of probability arising from interferences among coherently excited overlapping levels,[63] and the narrow structures may appear superimposed on a background arising from the broad resonances. If widths are extracted only for the narrow resonances, the average width may reflect a rate *smaller* than a statistical (e.g., RRKM) prediction.[61] Note that fluctuations in widths are also expected in dissociation from isolated (i.e., nonoverlapped) resonances,[71–73] however, the width of an isolated resonance can be assigned a rate, as per the uncertainty principle. Due to fluctuations, the decay width of a single resonance cannot be meaningfully compared with the prediction of a statistical theory.[19(c)]

A clear example of the effects of overlap on resonance widths is shown in Fig. 9. Comparing the R_{11}(7.5) spectrum (lower panel) with the Q_{11}(7.5) and R_{11}(6.5) spectra reveals a marked change in average resonance width. The R_{11}(6.5) spectrum displays numerous features of width (FWHM)<20 cm^{-1}; in contrast, no features *narrower* than ~25 cm^{-1} are observed in the R_{11}(7.5) spectrum. In this case, PHOFRY spectra for levels differing by a single J display gross changes in average resonance *width*. Note that the decay width of an isolated resonance, weakly bound to the continuum, cannot depend upon the particular channel monitored.[65]

To summarize the results obtained from double resonance IR–visible PHOFRY spectra at $E^{\dagger}$>2000 cm^{-1}, there exists no evidence of the strong correlations previously observed in one-photon PHOFRY spectra in the same energy region. On a global scale, *all* two-photon spectra exhibit marked differences in resonance structures, and poorer correlation. We note that some local similarities in resonance structures are always observed; the spectra are thus not to-

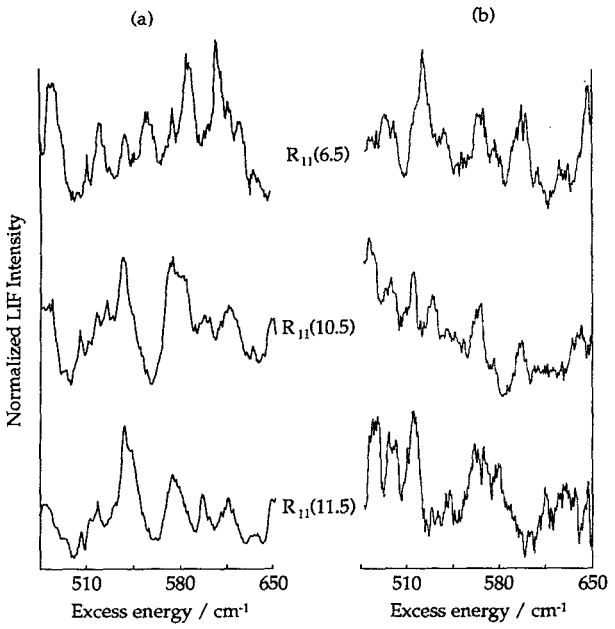

FIG. 10. (a) IR–visible PHOFRY spectra of NO_2 at $E^{\dagger}$=475–650 cm^{-1} obtained by monitoring the R_{11} (6.5), R_{11} (10.5), and R_{11} (11.5) transitions of the NO(0,0) band. (b) Visible–IR PHOFRY spectra for the same NO levels in the same energy region, obtained as described in the text.

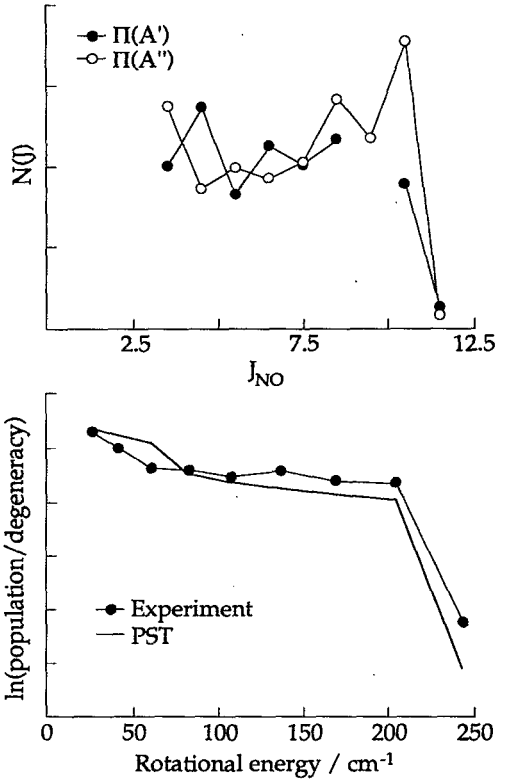

FIG. 11. NO($^2\Pi_{1/2}$) rotational state distributions at $E^{\dagger}$=235 cm^{-1} obtained using IR–visible excitation. The upper panel displays distributions in the two Λ-doublet states of NO; the lower panel compares in a Boltzmann plot the distribution summed over Λ-doublet levels with the prediction of PST.

tally uncorrelated. This is not surprising if we consider that each partial spectrum inherently arises from the same set of quasibound levels.

2. Visible–IR PHOFRY spectroscopy

We have obtained some visible–IR PHOFRY spectra as described in the experimental section of this paper. Displayed in Fig. 10(b) are three visible–IR spectra obtained by tuning the excitation laser to a peak at λ=441.177 nm and scanning the OPO over the region $E^{\dagger}$=475–650 cm^{-1} while probing NO(v=0) levels of J=6.5, 10.5, and 11.5. Like all previously viewed IR–visible spectra, these spectra are highly structured, and marked differences in resonance structures, positions, and widths are observed. Compare these spectra with those shown in Fig. 10(a), which displays three IR–visible PHOFRY spectra in the same energy region for the same NO(v,J,Λ,Ω) levels. PHOFRY spectra of identical levels for the two excitation schemes show marked differences in resonance structures. This is not unexpected, as the different intermediate levels accessed in the two experiments may have different Franck–Condon overlap with levels above dissociation threshold. It is likely that for both excitation schemes the $^2B_2$ state carries the oscillator strength in the second step.

C. NO($^2\Pi_{1/2}$,v=0) rotational state distributions obtained with IR–visible excitation

We have obtained some NO($^2\Pi_{1/2}$,v=0) rotational state distributions at $E^{\dagger}$<500 cm^{-1} using IR–visible excitation. Displayed in Figs. 11 and 12 are two distributions obtained at $E^{\dagger}$=235 and 400 cm^{-1}, respectively. The upper panel in each figure displays the distributions in the two (A', A'') (Ref. 48) Λ-doublet states of NO($^2\Pi_{1/2}$); the lower panel displays in a Boltzmann plot the sum of these distributions and the prediction of PST, as detailed in Ref. 17. Distributions obtained with one-photon excitation at these energies exhibit fluctuations which are largely suppressed when summing over Λ-doublet levels, and the summed distributions are in good agreement with PST.[10(a),10(b),17,21] This behavior is reproduced here; in fact, the Λ-doublet distributions in Fig. 11 (upper panel) display a distinct anticorrelation. However, comparison of Fig. 12 with Fig. 5 of Ref. 18(b) shows that distributions obtained at the same $E^{\dagger}$ with one- vs two-photon excitation display significantly different fluctuation patterns, as might be expected from the different set of quasibound levels accessed in the two experiments.

IV. DISCUSSION

A. The effective density of states above D_0: Implications for PHOFRY spectra

We have established previously the importance of overlapping quasibound levels in NO_2 decomposition.[18] The number of overlapped levels at a specific $E^{\dagger}$ is the product of the average decay width (Γ) and the density of states (ρ); for quantitative estimates of overlap, accurate values of Γ and ρ are needed. Recently, Ionov *et al.* examined the density of reactant levels in NO_2 decomposition through high resolution

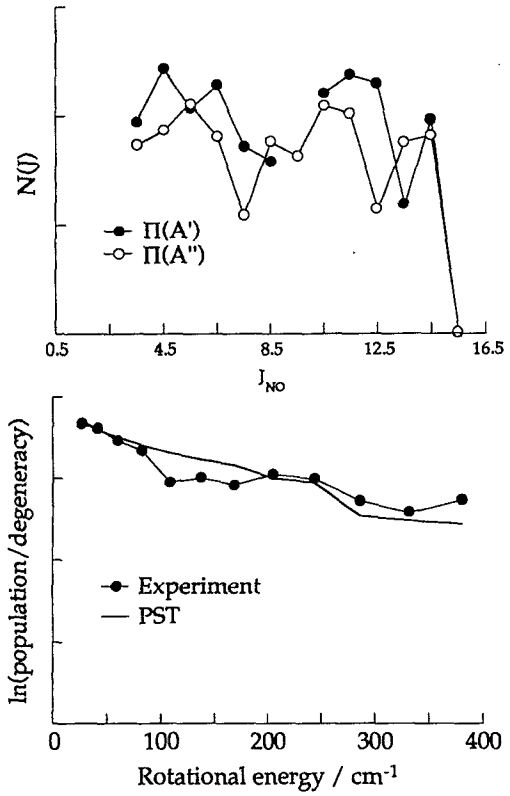

FIG. 12. NO($^2\Pi_{1/2}$) rotational state distributions at $E^\dagger$=400 cm^{-1} obtained using IR–visible excitation. The upper panel displays distributions in the two Λ-doublet states of NO; the lower panel compares in a Boltzmann plot the distribution summed over Λ-doublet levels with the prediction of PST.

fluorescence excitation spectra below threshold.[47] At energies of 0–60 cm^{-1} below D_0, 2–3 rovibronic levels per cm^{-1} of $J=1/2$ and 3/2 are observed on the average. This density primarily reflects rovibronic (i.e., Coriolis and spin–rotation) perturbations between optically bright B_2 vibronic levels and dark A_1 vibronic states,[44] although $^2A_2$ and $^2B_1$ electronic states may also contribute.[66–68] (Note that for IR–visible or visible–IR excitation the vibronic symmetry labels of bright and dark levels are reversed.) Above D_0, coupling to the NO+O continuum can modify the reactive density of states (ρ_{reac}); in a zeroth-order picture, coupling of a bright state to the continuum competes with coupling to dark levels.[47,69,70] Decay of the bright state describes the dynamics when coupling to the continuum dominates; ρ_{reac} is then a *vibronic* density of the bright B_2 (A_1 in double resonance experiments) states. If coupling to the continuum is weaker than rovibronic perturbations, ρ_{reac} may include the full rovibronic level density.

This simple picture, of course, does not address fluctuations in either rates[71–73] or rovibronic coupling matrix elements,[74] which will tend to obscure the transition between these limiting extremes. With this caveat, the implications of this discussion for our work center on the nature of structures observed in PHOFRY spectra and, more importantly, the *number* of overlapped levels as a function of energy. In the first 5 cm^{-1} above threshold, an average linewidth of ~0.15 cm^{-1} is obtained from the PHOFRY spectra of NO_2.[21] Recent experiments find an average matrix element for spin–rovibronic coupling of ~0.3 cm^{-1}.[74] This interaction is expected to be more significant, especially at low N, than Coriolis or centrifugal couplings. Here rovibronic perturbations are of similar magnitude to Γ, and therefore the full rovibronic state density is important in describing the dynamics. Note that even at threshold $\Gamma\sim 1/\rho$, which suggests that overlaps are expected (see Sec. IV B).

We may ask at what $E^\dagger$ the transition to a vibronic density of states takes place; some information is provided in the real-time measurements of Wittig and co-workers.[19] At $E^\dagger$>450 cm^{-1}, Γ is >3 cm^{-1}, or more than one order of magnitude larger than average spin–rotation coupling matrix elements. Here it seems reasonable to assume that the overlapping levels are *vibronic* (as opposed to rovibronic) in origin. The estimated A_1 vibronic state density in the threshold region is ~0.5 per cm^{-1}.[44,47] At $E^\dagger$=475–650 cm^{-1}, real-time measurements suggest Γ~3–6 cm^{-1},[19] and the levels overlap, but not severely. At $E^\dagger$=2000–2500 cm^{-1}, Γ~10–20 cm^{-1};[3(g),9,20] here, on the average, levels are more severely overlapped. This is relevant to differences in the correlations observed in IR–visible PHOFRY spectra in these two energy regions (see Sec. IV C).

B. Fluctuations from interference effects: Coherently excited overlapping quasibound levels and their evolution to final fragment states

On the average, we coherently excite several overlapped quasibound levels, and interferences among them are expected. However, we must also examine the projection of these states onto the vibrational levels of the TS and their subsequent evolution to products. As a framework, we use scattering matrix formalism.[75–78] Eigenstates near dissociation threshold are predominantly of mixed $^2B_2/^2A_1$ electronic character,[26–44] and a basis set of $^2B_2$ and $^2A_1$ vibronic states must therefore be used to represent an isolated (ergodic) quasibound level $|\Psi_R\rangle$,[79]

$$|\Psi_R\rangle=\sum_s c_s|\Psi_s\rangle+\sum_l c_l|\Psi_l\rangle, \tag{1}$$

where $|\Psi_s\rangle$ represents a zeroth-order optically bright $^2B_2$ state and $|\Psi_l\rangle$ a dark $^2A_1$ state. For one-photon excitation, $|\Psi_R\rangle$ has B_2 vibronic symmetry; IR–visible or visible–IR excitation prepares $|\Psi_R\rangle$ of A_1 vibronic symmetry. The transition dipole matrix element connecting an *isolated* quasibound level with initial state i in the electronic ground state is given by

$$R_{iR}=\langle\Psi_i|\mu_{iR}|\Psi_R\rangle f(E,E_R), \tag{2}$$

$f(E,E_R)$ has the form[50,51]

$$f(E,E_R)\propto\frac{1}{(E-E_R)+(i\Gamma_R/2)}, \tag{3}$$

where E_R is the resonance energy and

$$\Gamma_R=\sum_f \Gamma_{Rf} \tag{4}$$

is the sum of partial widths into all channels f. Here Γ_R is the "true" decay width, which is directly related to the decomposition lifetime via the uncertainty principle. Since $\langle\Psi_i|\mu_{il}|\Psi_l\rangle \equiv 0$, Eq. (2) reduces to

$$R_{iR} \propto \sum_s c_s \langle\Psi_i|\mu_{iS}|\Psi_S\rangle f(E,E_R). \tag{5}$$

We now consider projection of one or more excited quasibound level(s) onto the manifold of fragment states via the TS, and discuss two limiting cases; (i) dissociation near threshold, where the TS is loose and the TS levels are approximately those of a free NO rotor, and (ii) dissociation at the energies accessed in our experiments, i.e., >200 cm^{-1} above threshold, where the TS has significantly tightened.

1. Dissociation just above threshold

As shown by Miyawaki *et al.*,[21] just above threshold the TS is loose (PST-like), and its levels are thus approximately those of the free fragments, including degeneracies. For decay of an isolated quasibound level via a loose TS, the cross section $\sigma_{f\leftarrow i}$ for formation of final state f from initial parent state i is

$$\sigma_{f\leftarrow i} \propto |R_{iR}\langle R|S_{Rf}|f\rangle|^2, \tag{6}$$

where $\langle R|S_{Rf}|f\rangle$ is the scattering matrix element to final asymptotic state f [for NO_2 near threshold, $f=NO(^2\Pi_{1/2};J,\Lambda)+O(^3P_2)$]. Decay via a single quasibound level may evidence fluctuations in level populations in the f-manifold,[49,65] which should be significantly damped when averaging over several initial states, or when several resonances are incoherently accessed.

We now consider projection of several *coherently excited* overlapping quasibound levels onto the f state manifold via a loose TS. Following Eq. (6),

$$\sigma_{f\leftarrow i} = \left| \sum_R R^*_{iR}(e^{i\varphi_R})\langle R|S_{Rf}|f\rangle \right|^2. \tag{7}$$

Equation (7) incorporates the square of a sum over quasibound levels, where in the complex coefficients the phases are explicitly assigned, and the cross terms represent the interferences. Consistent with the independence hypothesis, we assume that the R^*_{iR} and the $\langle R|S_{Rf}|f\rangle$ are uncorrelated and that formation and decay of the excited complex can be separated. This is physically reasonable, since near threshold NO_2 decomposes on a time scale of several picoseconds,[3(g),9,19,21] or many vibrational periods. To illustrate the effect of interfering amplitudes on state-specific PHOFRY spectra, we have carried out calculations based on the formalism of Eq. (7). In our calculations, the positions (E_R) of the quasibound levels are randomly distributed within a specified energy range according to a Wigner distribution of nearest neighbor level spacings,[34,44] and the average density of resonances (ρ) is the one given in Sec. IV A. The excitation probabilities (i.e., the $\langle i|\mu_{iR}|R\rangle$) are chosen as uniform random deviates between 0 and 1. For the distribution of decay widths (Γ_R) we use a chi-square distribution with n degrees of freedom,[71,72] where n is the number of independent decay channels. For simulations of spectra near threshold, n is

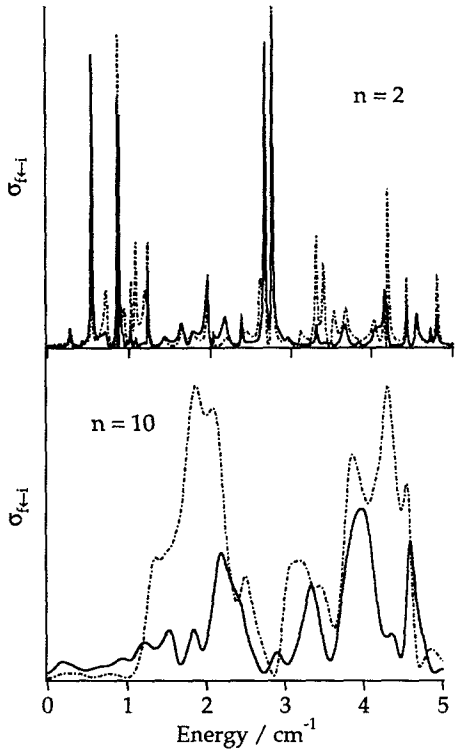

FIG. 13. Mock PHOFRY spectra which illustrate the spectral manifestation of the transition from weak ($\Gamma\rho<1$, upper panel) to stronger ($\Gamma\rho>1$, upper panel) level overlap. The quasibound level density is 10/cm^{-1}.

counted according to phase space theory (PST). At higher energies where the TS has tightened, n is the number of states of the TS and is taken from variational RRKM calculations.[20] RRKM behavior is explicitly assumed by equating n, ρ, and Γ according to the familiar RRKM expression, written in terms of the more common rate $k(E)$,

$$\Gamma = \hbar k(E) = \frac{N^\dagger(E^\dagger)}{2\pi\rho} = \frac{n}{2\pi\rho}, \tag{8}$$

where $N^\dagger(E^\dagger)$ represents the number of states of the TS which are energetically available at excess energy $E^\dagger$. The line shape function $f(E,E_R)$ used in our calculations is that shown in Eq. (3). These parameters are fixed as input to calculate $\sigma_{i\rightarrow f}$, while the phases of the resonances (φ_R) and the $\langle R|S_{Rf}|f\rangle$ are chosen as uniform random deviates in the intervals $0-2\pi$ and 0–1, respectively, and are changed from run to run. Sequences of random deviates are generated via functions obtained in Refs. 80 and 81. As an initial exercise, we illustrate the effect of increasing level overlap with the simulated spectra shown in Fig. 13. Here the degree of overlap, defined by $\Gamma\rho$ and equal to $n/2\pi$ from Eq. (8), is varied by a factor of 5 between the upper and lower panels. The increasing difference between the two individual (random) weightings shown in each panel is apparent.

Before continuing, we need to emphasize that the goal of these numerical experiments is not to achieve *quantitative* agreement with the measured PHOFRY spectra; this would require detailed knowledge of the molecular Hamiltonian

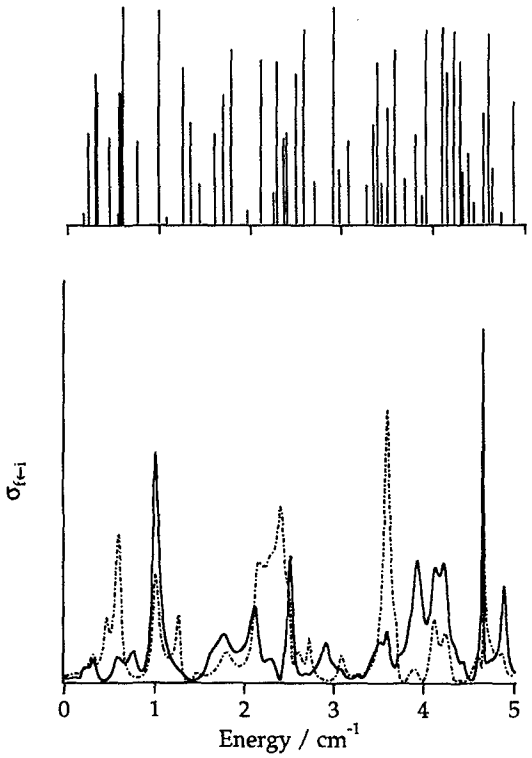

FIG. 14. Mock PHOFRY spectra in the region 0–5 cm^{-1} above threshold. This calculation included a quasibound level density of 10/cm^{-1}, an average width of 0.13 cm^{-1}, and 4 open channels. The positions and relative intensities of the underlying quasibound levels are shown in the upper panel. Each displayed spectrum represents a different (random) weighting of the complex coefficients of the underlying quasibound levels.

and explicit incorporation of all couplings. Rather, our intention is to examine the sources of the fluctuations and determine if qualitative features of the spectra (e.g., the final state dependence of line positions, intensities, shapes, and widths) can be reproduced. Where possible, we have used parameters appropriate for NO_2 taken from a variety of experimental and theoretical data. Although these parameters are often not accurately known, we believe that our chosen values are accurate to within a factor of 2.

We now discuss the validity of the assumptions of and inputs into the model. First, our calculations do not include details of the relevant potential energy surface(s); for example, no anisotropies or final state interactions are included. Second, the quasibound levels are ascribed a width that reflects their coupling to the continuum; however, no account of interactions between these levels via their common interaction with the continuum is included. Finally, the use of random phases and amplitudes in the construction of overlapped resonances is arbitrary and reflects our ignorance of more specific criteria.

The lower panel of Fig. 14 exhibits two mock PHOFRY spectra of the region 0–5 cm^{-1} above threshold in NO_2. Each spectrum results from a different (random) weighting of the φ_R and the $\langle R|S_{Rf}|f\rangle$. The number of quasibound levels reflects the level density (~10 states/cm^{-1} of $J=1/2$ and 3/2) observed by Ionov *et al.* in the range 0–5 cm^{-1} below

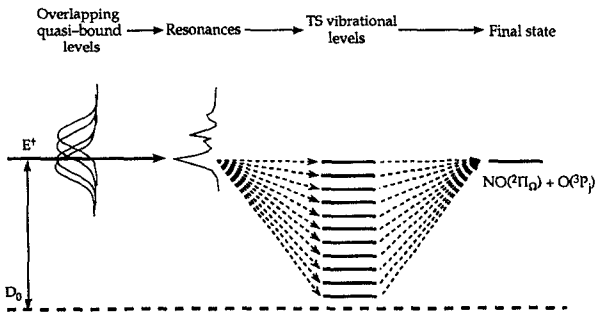

FIG. 15. Schematic of the NO_2 dissociation mechanism. At a specific $E^\dagger$, several overlapping quasibound levels are coherently excited. Interferences among these levels produce resonance structures, which are (randomly) projected onto the accessible levels of the tight TS. The TS levels, in turn, map onto specific sets of NO quantum states. Projection through multiple TS levels gives rise to interferences.

threshold;[47] the upper panel displays the positions and relative intensities of these levels. Here we set $n=4$ in the chi-square distribution, since although only two channels are energetically accessible {NO[$^2\Pi_{1/2}$, $v=0$, $J=0.5$, Λ; $\Lambda=\Pi(A'')$, $\Pi(A')$]+O($^3P_2$)}, the number of TS levels $N^\dagger(E^\dagger)$ counted using PST is 4.[21] Using these parameters, Γ is calculated according to Eq. (8), and $\Gamma\rho=0.64$.

The calculated spectra resemble, in a qualitative way, the experimental PHOFRY spectra. First, in both experiment and calculations the number of observed peaks is much smaller than the number of underlying levels (i.e., ~10 vs 50).[21] Second, and more importantly, the experimental PHOFRY spectra for the two Λ-doublet states of NO ($v=0$, $J=0.5$) clearly display differences in the resonance structures.[21] Similarly, the calculations also show changes in peak widths, shapes, positions, and amplitudes for different weightings of the phases and coefficients of the quasibound levels.

2. Dissociation at higher $E^\dagger$

We now consider decomposition at higher excess energies (i.e., >200 cm^{-1}). Here the TS has tightened significantly, as observed in real-time measurements of $k(E)$ (Ref. 19) and predicted by variational RRKM calculations.[20] Also, as the lifetime decreases with increasing $E^\dagger$, on the average the decay widths of the quasibound states increase and more levels overlap. The cross section may be written as

$$\sigma_{f\leftarrow i}\propto\left|\sum_R\sum_n R_{iR}A_{Rn}\langle n|S_{nf}|f\rangle\right|^2, \tag{9}$$

where A_{Rn} is the amplitude of projection of quasibound level R onto TS level n, and the S-matrix elements now connect each TS level n to product level f. This model, represented schematically in Fig. 15, assumes that coherently excited overlapping quasibound states decay through multiple vibrational levels of the TS. We also assume that the R_{iR}, A_{Rn}, and $\langle n|S_{nf}|f\rangle$ are uncorrelated and can be treated independently; we thus replace the double sum with a single sum over n, and include in A_{R^*n} all the terms describing the excitation of specific overlapped resonances. The cross section is then written as

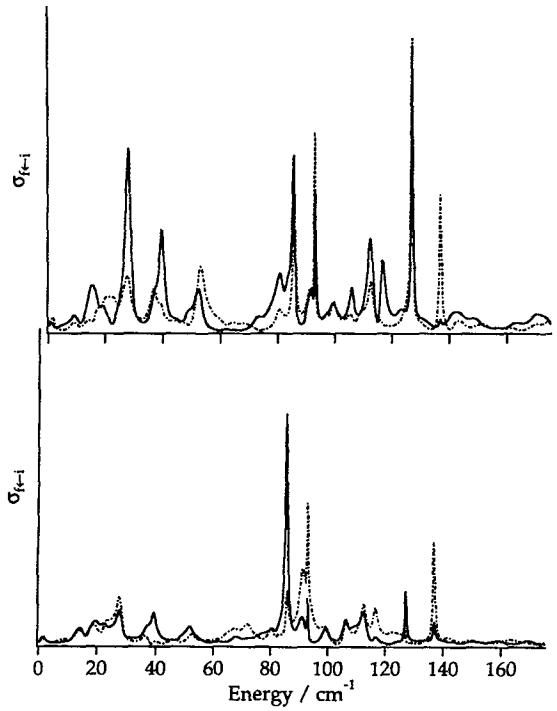

FIG. 16. Mock PHOFRY spectra in the region $E^{\dagger}=475-650$ cm^{-1}. This calculation included a quasibound level density of 0.44/cm^{-1}, an average width of 4 cm^{-1}, and 11 open channels. Each displayed spectrum represents the sum of three different (random) weightings of the complex coefficients of the underlying quasibound levels.

$$\sigma_{f\leftarrow i}\propto\left|\sum_{n} A_{R^*n}\langle n|S_{nf}|f\rangle\right|^2. \tag{10}$$

In describing the projection of the resonances (which are composed of chaotic quasibound states) onto the final state manifold via the TS, we assume a random weighting of TS levels (i.e., random A_{R^*n}). Due to the rapid passage from the TS to products, we also assume that the evolution of TS wave functions into final product states is sudden (see below).

To illustrate the contributions from the different components of this model, we carried out two sets of separate calculations, one involving the projection of the quasibound states onto the TS and the other the evolution of the TS wave functions to final product states. First, we examined effects from increasing level overlap by using Eq. (7) and substituting n for f. We considered the two regions where we obtained most of the experimental results, $E^{\dagger}=475-650$ cm^{-1} and 2000–2500 cm^{-1}. At $E^{\dagger}=475-650$ cm^{-1}, an experimental correlation is observed on the basis of J [Fig. 5 and Fig. 3 of Ref. 18(a)]; a much poorer correlation on this basis is observed in spectra at $E^{\dagger}=2000-2525$ cm^{-1}. A clear difference between these two regions is the degree of average homogeneous lifetime broadening, which increases from ~3–6 cm^{-1} to ~10–20 cm^{-1}.[3(g),9,20] Assuming a state density <1.0 per cm^{-1} (see Sec. IV A), these regions correspond to regimes of mild ($\Gamma\geqslant 1/\rho$) and more severe overlaps. To model this effect, we display in Fig. 16 four mock PHOFRY spectra calculated using parameters appropriate for the lower energy region. Specifically, we use an average quasibound level width of 4 cm^{-1},[3(g),9,19] and $n=11$.[20] Figure 17 displays four mock PHOFRY spectra appropriate for the region $E^{\dagger}=2000-2500$ cm^{-1} obtained using an average width of 15 cm^{-1},[3(g),9,19] and $n=20$.[20] In both cases ρ is calculated using Eq. (8). Each displayed spectrum in Figs. 16 and 17 represents the sum of three individual (random) weightings; this provides a more realistic description of the experiment, since three spin–orbit states in the $O(^3P_j;\ j=2,1,0)$ fragment are inherently correlated with each NO level. Comparing the spectra in Figs. 16 and 17, we notice that the former exhibit significantly better reproduction (in terms of shapes, positions, and widths) of resonance structures, due to the smaller degree of level overlap. While many features of these simulated spectra are also observed in the experiment, we note that these simulations cannot be directly compared with the experimental results because they do not take into account the evolution of the system from the TS to final products (see below).

In describing the projection of the overlapped resonances onto the TS, we implicitly assume a random weighting of TS levels. In a separate set of calculations, we treated the evolution of the TS wave function into final product states by using a set of harmonic oscillator TS basis wave functions *whose complex coefficients are randomly weighted.*

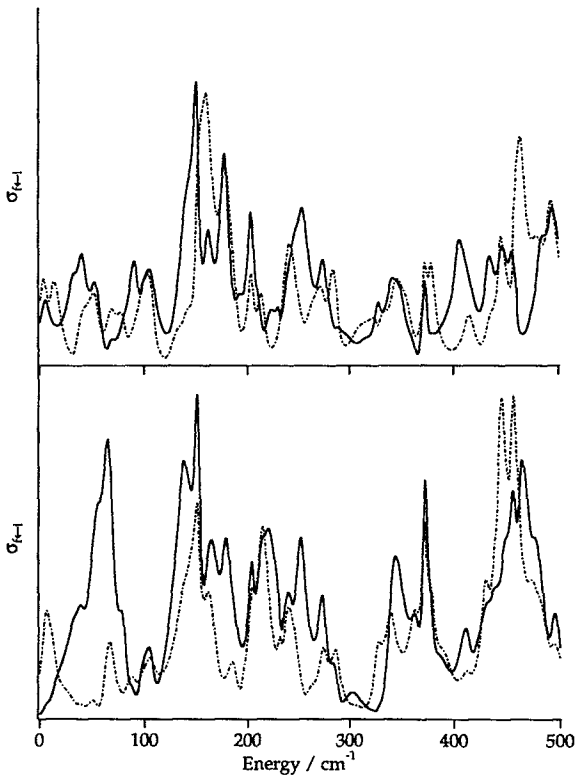

FIG. 17. Mock PHOFRY spectra in the region $E^{\dagger}=2000-2500$ cm^{-1}. This calculation included a quasibound level density of 0.21/cm^{-1}, an average width of 15 cm^{-1}, and 20 open channels. Each spectrum results from a superposition of three different (random) weightings of the coefficients and phases of the quasibound levels.

As a limiting case, we use the Franck–Condon (FC) model for dissociation as described in Refs. 82–84. In these calculations we use the formalism of Gelbart and Beswick[83] and Jacobi coordinates,[65] and assume that the evolution of the bending-like TS wave functions into product states is sudden, and that no exit-channel interactions are important beyond the TS. The number of transition state levels (20), and location of the TS ($R=2.2$ Å) are obtained from the calculations of Ref. 20. A TS Jacobi angle (γ) of 130° and bending width of 20° are chosen from Refs. 20 and 25. The TS wave function is taken as a linear combination of harmonic oscillator wave functions, weighted with random coefficients (magnitude=0–1) and phases (magnitude=0–2π), i.e.,

$$\Psi=\sum_i c_i e^{i\varphi_i}\psi_i(\theta). \tag{11}$$

At $E^{\dagger}>2000$ cm^{-1}, where many of the rotational state distributions were obtained,[17] the use of bending-like wave functions to represent the TS levels is justified;[19,20] for computational ease we treat these levels as harmonic. Rotational level distributions calculated by expanding the TS wave function into a basis set of spherical harmonic (i.e., NO free rotor) wave functions are smoothed via 5-point smoothing to reduce fast oscillations which are expected to wash out experimentally.[84–86]

Figure 18 displays the results of two calculations using this method and two experimental NO distributions obtained with one-photon excitation at $E^{\dagger}=2061$ and 3038 cm^{-1}, respectively, as reported in Ref. 17(b). Each experimental NO distribution is summed over the individual Λ-doublet state distributions; recall that, at these energies, this does not dampen the oscillatory patterns.[18] We have used data obtained with one-photon excitation because the incoherent superposition over several parent rotational levels smoothes over some of the fast fluctuations and better reveals the oscillatory structures (see also Sec. IV C). We must again emphasize that these calculations are not intended to *simulate* the experimental distributions, but merely to show that distributions similar to those observed experimentally (i.e., oscillatory structures that depend sensitively on the excited resonance) may be produced within the framework of this model. The calculated distributions shown in Fig. 18 were chosen from a large number of distributions simply because of their remarkable resemblance to the experiment. Like the experiment, calculations produce highly structured rotational distributions which vary sensitively for different weightings; some weightings produce more PST-like distributions, others produce prominent oscillatory structures of the type shown in Fig. 18. We find that our ability to produce structured distributions that vary randomly for each sampling depends on the inclusion of phase, and thus the presence of interference. A simple superposition of positive amplitudes does not successfully reproduce this effect; however, the exact distribution of phases is not important.

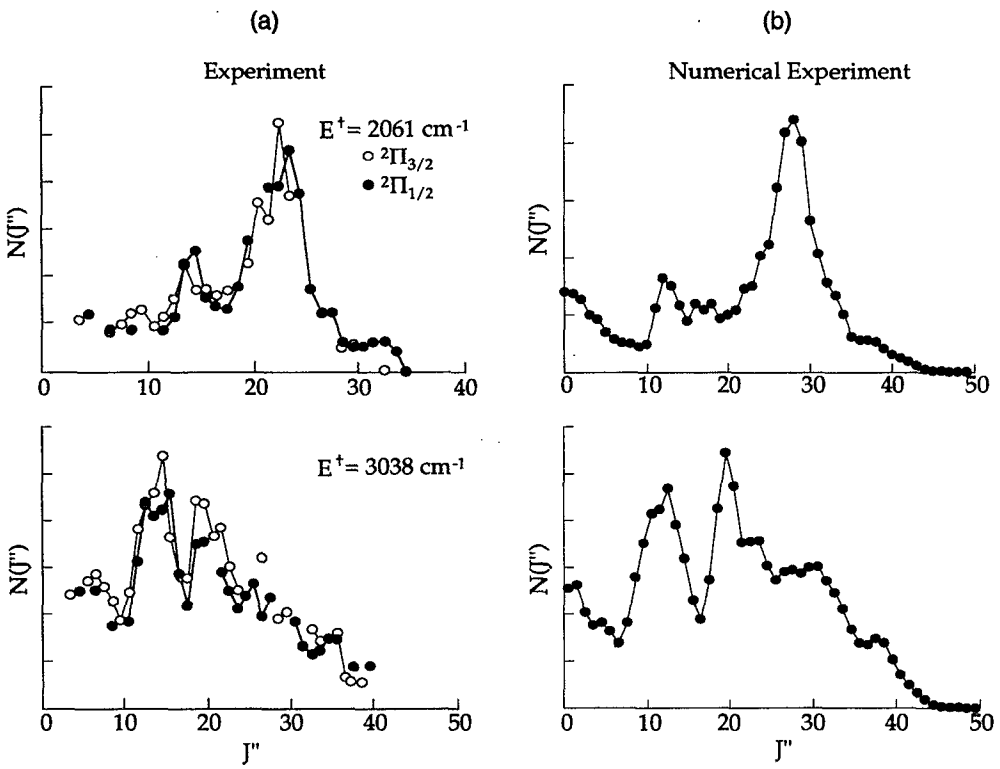

FIG. 18. (a) NO($^2\Pi_{1/2}$) and ($^2\Pi_{3/2}$) rotational state distributions in $v=0$ at $E^{\dagger}=2061$ and 3038 cm^{-1}, obtained using one-photon excitation. (b) Calculated distributions using the Franck–Condon expansion of sets of harmonic oscillator wave functions whose coefficients and phases are randomly weighted, as described in the text. This figure highlights the similarity between distributions obtained in the experiment and in sample calculations.

The simple calculations described above succeed in simulating (in a qualitative way) many features observed in the experiments. First, we obtain highly structured, but on the average "statistical" (i.e., PST-like), rotational state distributions. Second, the simulated distributions sensitively depend on the weightings of the TS levels [Eq. (11)], which in turn depend (via projections) on weightings of the quasibound levels in the excited resonance state. The calculated distributions therefore vary significantly over small ranges of energy, as also observed experimentally.[17] Third, interferences among the overlapping levels are observed in both experimental and simulated PHOFRY spectra as resonance structures which sensitively depend upon weightings of the overlapped quasibound states. We note, however, that in the experiments the observed relative population of a specific final NO state is a result of the full projection of the excited resonance onto that state, which is a convolution of the two sets of the simulations described here. More detailed recent calculations, which combine the two sets of simulations described above in an effective Hamiltonian formalism, reproduce (in a qualitative way) the spectra and rotational state distributions obtained with the simple model described here.[64]

It is instructive to examine how the results of the present model relate to a statistical description of unimolecular reactions. The picture of overlapping resonances has previously been invoked in the description of complex decomposition,[50–55,76] and shown to lead to shifts in spectral positions and to fluctuations in the partial absorption cross sections and widths. The connection to RRKM theory has been discussed by several authors;[63,71,76] however, a definitive picture has not yet emerged. Fluctuations in widths have been treated in detail for the case of isolated (i.e., non overlapped) resonances.[69,71–73]

Oscillatory structures and fluctuations in product state distributions have not previously been treated within the framework of statistical theories. The model we present predicts fluctuations in the rotational distributions at low excess energies where the TS is very loose, and this agrees with experimental observations. The appearance of larger oscillatory structures at higher excess energies is associated with a tighter TS and, in the limit of no final state interactions beyond the TS, with mappings of *bending-like* TS wave functions into free-rotor product states. It is intriguing that PST-like rotational distributions are obtained on average even with a tight TS. This may not be too surprising if we recall that the range of rotational excitations in FC mapping depends on the TS bending angle and frequency. For NO_2, the TS parameters obtained from calculations lead to rotational distributions that span the full range allowed by energy conservation at excess energies up to 3000 cm^{-1}. Also, as the TS tightens with increasing excess energy, the bending frequency increases,[20] leading to an increase in rotational excitation with excess energy.[65,85] Thus, the good agreement obtained with PST even at high excess energies may reflect the specific geometry of the TS.

The assumption of no final state interaction beyond the TS at high excess energy cannot be tested experimentally at present. It is reasonable to imagine that as the excess energy increases and the dissociation becomes more rapid, the probability for rotational energy transfer in the exit channel will decrease, at least for high rotational levels. It is also plausible that the fast evolving fragments may follow the diabatic, rather than the adiabatic, curves at high excess energy, and this may occur more frequently for the low rotational levels whose recoil velocities are larger. Thus, it is likely that at relatively low excess energies (e.g., $E^{\dagger}\sim500$ cm^{-1}) energy transfer among rotational states in the exit channel will smooth over oscillations and fluctuations, while at the higher excess energies ($E^{\dagger}>2000$ cm^{-1}) the oscillatory structures resulting from mapping of the TS wave functions are more likely to be observed. This may contribute to the experimental observation that IR–visible PHOFRY spectra at low excess energies are better correlated than those at the higher $E^{\dagger}$. More experimental and theoretical work is needed to explore the importance of the long-range interactions beyond the TS.

C. Implications of IR–visible PHOFRY spectra: Comparisons of one- and two-photon experiments

Both IR–visible and visible–IR PHOFRY spectra exhibit resonance structures that sensitively depend on the monitored NO level and fluctuate from channel to channel, with no evidence at higher $E^{\dagger}$ of the strong correlations previously observed in one-photon spectra.[18(b)] Two factors must be considered in comparing one- and two-photon experiments; (i) the different symmetry species (either vibronic or rovibronic) optically accessed in the two experiments, and (ii) the greater degree of initial state selection in the two-photon experiments.

The level densities of symmetry species accessed in one- vs two-photon experiments bears on the *average number* of overlapping levels coherently excited as a function of energy. For two-photon excitation, optically bright levels are of A_1 vibronic symmetry, arising from the mixing of b_2 vibrational levels in the $^2B_2$ state with a_1 vibrational levels in the ground $^2A_1$ state. Extrapolation of level densities at lower energies yields a B_2 vibronic state density of $\sim$0.5 per cm^{-1} in the threshold region;[47] the A_1 level density should be similar, since zeroth-order a_1/b_2 vibrational levels differ only in quanta (i.e., even vs odd) of asymmetric stretching excitation. On an energy scale large with respect to local fluctuations in state density, one- and two-photon experiments should not show pronounced differences on this basis; i.e., the average number of *coherently* excited overlapped levels at a specific $E^{\dagger}$ should be similar.

Consider now the greater degree of parent state selection in the two-photon experiment. At energies where our comparisons are made, i.e., $E^{\dagger}=2000$–2500 cm^{-1}, the average decay width is $\sim$15–20 cm^{-1}, significantly larger than the rotational envelope of a vibronic band at $\sim$5 K. One-photon excitation from *different* parent rotational levels thus accesses primarily the *same* set of overlapped vibronic quasibound states, with relative intensities determined by line strength factors. Excitation from a single parent rotational level *coherently* accesses these levels, and interferences produce the resonance structures we have discussed. If the weightings of the quasibound levels are slightly different for different parent rotational levels, the resulting resonance

structures may be shifted in energy for each coherent superposition. Excitation from *different* parent levels is *incoherent*, and thus the observed spectrum, which is a superposition of spectra from different levels, may be broadened. This may explain why more narrow features are observed in two- vs one-photon PHOFRY spectra at these energies, and partially account for the more pronounced final state dependence of two-photon PHOFRY spectra.

We next consider projection of resonance structures onto the TS. Based on the preceding argument, the weighting of TS levels in one-photon experiments is a superposition of several weightings *with (possibly) similar coefficients but different phases*. We have examined this effect in our calculations by using wave functions weighted with the same (random) coefficients but different sets of (random) phases. In comparing distributions obtained for individual runs with those obtained by superimposing several runs, we find the effect of superposition to be the reduction, but not elimination, of fast oscillations in the distributions. The same conclusion is reached in calculations that vary the coefficients as well as phases of the TS wave functions. This dampening of fast oscillations resulting from superpositions may also contribute to differences in correlations observed in two- vs one-photon PHOFRY spectra. With increasing numbers of superpositions (i.e., when simulating the effect of 300 K excitation), the distributions become quite smooth, in agreement with the smooth, PST-like behavior obtained experimentally with room temperature samples.[11,22]

V. SUMMARY AND CONCLUSIONS

We have examined fluctuations in the unimolecular decomposition of NO_2 through detailed double resonance experiments and sample calculations. The primary findings of this work are as follows:

(1) All IR–visible PHOFRY spectra at $E^{\dagger}=2000$–2525 cm^{-1} exhibit marked differences in the shapes, positions, and widths of resonance structures. We interpret this as arising from interference effects among overlapping quasibound levels. Qualitative trends in these spectra are reproduced in sample calculations based on scattering matrix formalism. Unlike one-photon PHOFRY spectra in the same energy region, no clear correlations are apparent. This is ascribed to the greater degree of parent state selection in two-photon experiments, which reduces superpositions due to incoherent excitation from different parent rotational levels.

(2) In many of the IR–visible PHOFRY spectra, we observe features significantly narrower than expected from consideration of average decomposition lifetimes. We also see marked changes in average resonance width for spectra obtained by monitoring different NO levels. These effects are consistent with interferences among overlapping quasibound levels.

(3) A correlation based on J observed in IR–visible PHOFRY spectra at $E^{\dagger}=475$–650 cm^{-1} is much poorer at higher $E^{\dagger}$. As shown in sample calculations, this may arise from the more severe degree of level overlap in the higher energy region.

(4) Visible–IR PHOFRY spectra show the same general trends, but display significantly different resonance structures. This is expected from consideration of the different intermediate levels accessed in the two experiments.

(5) Consistent with the model previously proposed,[18] we have shown, in a second set of illustrative calculations, that highly structured, but on the average statistical (i.e., PST-like), rotational state distributions can be obtained in Franck–Condon expansions of sets of harmonic oscillator wave functions whose coefficients and phases are randomly weighted.

A rather complete picture of the unimolecular decomposition of NO_2 emerges from the frequency and time domain studies. At all energies, overlapping quasibound levels are the rule rather than the exception; however, the degree of overlap is not severe. The effects of interference among overlapped levels is manifested most strongly in PHOFRY spectra. We have shown, in sample calculations, that due to interferences, a pronounced dependence of resonance positions, shapes, and widths on the weighting of the quasibound levels is obtained. In addition, interferences can produce resonance structures significantly narrower than the average decay width.[75(c)] We assume that the TS levels accessed in the evolution of the resonances to product states are weighted with random complex coefficients. Evidence from both frequency[21] and time domain[19] experiments, and variational RRKM calculations[20] indicates that the TS moves in along the reaction coordinate with increasing $E^{\dagger}$. At $E^{\dagger}\sim 2000$ cm^{-1}, the TS has significantly tightened,[20] and we approximate its levels by bending-like harmonic oscillator wave functions. We have reproduced the oscillatory structures in the rotational distributions using Franck–Condon mappings of sets of harmonic oscillator TS wave functions whose coefficients and phases are randomly weighted, assuming no final state interactions beyond the TS. This assumption becomes more valid with increasing $E^{\dagger}$. These calculations show that PST-like distributions may be obtained for specific geometries of the TS without the primary assumption of PST, namely, a "loose" TS. At yet higher energies, when the decay rate becomes even faster, a direct dissociation channel may become significant.[10(b)]

To conclude, we note that the study of NO_2 decomposition provides a unique opportunity to view the underlying causes of statistical behavior. Specifically, we see in the fluctuations and oscillatory structures how deviations from traditional statistical theories are first manifested, and through these observables are able to test some assumptions of these models. Although our level of understanding of NO_2 decomposition is rapidly converging, it will continue to remain an important system for refining our understanding of barrierless unimolecular decomposition.

ACKNOWLEDGMENTS

The authors wish to thank R. Schinke for providing the program used in the Franck–Condon calculations, and gratefully acknowledge many useful discussions with or receipt of preprints from C. Wittig, H. S. Taylor, R. Schinke, S. I.

Ionov, D. C. Robie, M. Hunter, L. A. Harding, J. Troe, C. B. Moore, W. H. Miller, U. Peskin, K. Yamanouchi, S. Tsuchiya, S. J. Klippenstein, R. Jost, P. L. Houston, and R. D. Levine. This research was supported by the National Science Foundation and the U.S. Army Research Office.

[1] P. J. Robinson and K. A. Holbrook, *Unimolecular Reactions* (Wiley, New York, 1972); W. Forst, *Theory of Unimolecular Reactions* (Academic, New York, 1973); K. J. Laidler, *Theories of Chemical Reaction Rates* (MacGraw–Hill, New York, 1979); D. M. Wardlaw and R. A. Marcus, Adv. Chem. Phys. **70**, 231 (1988), and references therein.

[2] P. Pechukas, J. C. Light, and C. Rankin, J. Chem. Phys. **44**, 794 (1966); P. Pechukas and J. C. Light, *ibid.* **42**, 3281 (1965); J. C. Light, Discuss. Faraday Soc. **44**, 14 (1967).

[3] (a) M. Quack and J. Troe, Ber. Bunsenges. Phys. Chem. **78**, 240 (1974); (b) **79**, 171 (1974); (c) **79**, 469 (1975); (d) **81**, 329 (1977); (e) J. Troe, J. Chem. Phys. **66**, 4758 (1977); (f) **75**, 226 (1981); (g) **79**, 60 (1983); (h) J. Phys. Chem. **83**, 114 (1979).

[4] C. X. W. Qian, M. Noble, I. Nadler, H. Reisler, and C. Wittig, J. Chem. Phys. **83**, 5573 (1985), and references therein; C. Wittig, I. Nadler, H. Reisler, M. Noble, J. Catanzarite, and G. Radhakrishnan, *ibid.* **83**, 5581 (1985); H. Reisler and C. Wittig, Annu. Rev. Phys. Chem. **37**, 307 (1986), and references therein; H. Reisler and C. Wittig, in *Advances in Kinetics and Dynamics*, edited by J. R. Barker (JAI, Greenwich, 1992), Vol. 1.

[5] (a) L. R. Khundkar, J. L. Knee, and A. H. Zewail, J. Chem. Phys. **87**, 77 (1987); (b) S. J. Klippenstein, L. R. Khundkar, A. H. Zewail, and R. A. Marcus, *ibid.* **89**, 4761 (1988).

[6] W. H. Green, Jr., C. B. Moore, and W. F. Polik, Annu. Rev. Phys. Chem. **43**, 307 (1992); W. H. Green, I.-C. Chen, and C. B. Moore, Ber. Bunsenges. Phys. Chem. **92**, 389 (1988); I.-C. Chen, W. H. Green, and C. B. Moore, J. Chem. Phys. **89**, 314 (1988).

[7] S. J. Klippenstein and R. A. Marcus, J. Chem. Phys. **91**, 2280 (1989).

[8] G. E. Busch and K. Wilson, J. Chem. Phys. **56**, 3626 (1972); **56**, 3638 (1972).

[9] H. Gaedtke and J. Troe, Ber. Bunsenges. Phys. Chem. **79**, 184 (1975); M. Quack and J. Troe, *ibid.* **79**, 469 (1975); H. Gaedtke, H. Hippler, and J. Troe, Chem. Phys. Lett. **16**, 177 (1972).

[10] (a) U. Robra, H. Zacharias, and K. H. Welge, Z. Phys. D **16**, 175 (1990); (b) U. Robra, Ph.D. thesis, University of Bielefeld, 1984; (c) H. Zacharias, M. Geilhaupt, K. Meier, and K. H. Welge, J. Chem. Phys. **74**, 218 (1981); (d) H. Zacharias, K. Meier, and K. H. Welge, in *Energy Storage and Redistribution in Molecules*, edited by J. Hinze (Plenum, New York, 1983).

[11] M. Mons and I. Dimicoli, Chem. Phys. Lett. **131**, 298 (1986); Chem. Phys. **130**, 307 (1989).

[12] M. Kawasaki, H. Sato, A. Fukuroda, T. Kikuchi, S. Kobayashi, and T. Arikawa, J. Chem. Phys. **86**, 4431 (1987).

[13] K. Chen and C. Pei, Chem. Phys. Lett. **137**, 361 (1987).

[14] H.-G. Rubahn, W. J. van der Zande, R. Zhang, M. J. Bronikowski, and R. N. Zare, Chem. Phys. Lett. **186**, 154 (1991).

[15] (a) J. Miyawaki, T. Tsuchizawa, K. Yamanouchi, and S. Tsuchiya, Chem. Phys. Lett. **165**, 168 (1990); (b) J. Miyawaki, K. Yamanouchi, and S. Tsuchiya, *ibid.* **180**, 287 (1991); (c) K. Yamanouchi, S. Takeuchi, and S. Tsuchiya, J. Chem. Phys. **92**, 4044 (1990).

[16] P.-A. Elofson and E. Ljungstrom, Chem. Phys. **165**, 323 (1992).

[17] (a) D. C. Robie, M. Hunter, J. L. Bates, and H. Reisler, Chem. Phys. Lett. **193**, 413 (1992); (b) M. Hunter, S. A. Reid, D. C. Robie, and H. Reisler, J. Chem. Phys. **99**, 1093 (1993).

[18] (a) S. A. Reid, J. T. Brandon, M. Hunter, and H. Reisler, J. Chem. Phys. **99**, 4860 (1993); (b) S. A. Reid, D. C. Robie, and H. Reisler, *ibid.* **100**, 4256 (1994).

[19] (a) G. A. Brucker, S. I. Ionov, Y. Chen, and C. Wittig, Chem. Phys. Lett. **194**, 301 (1992); (b) S. I. Ionov, G. A. Brucker, C. Jaques, Y. Chen, and C. Wittig, J. Chem. Phys. **99**, 3420 (1993); (c) C. Wittig and S. I. Ionov, *ibid.* **100**, 4717 (1994).

[20] S. J. Klippenstein and T. Radivoyevitch, J. Chem. Phys. **99**, 3644 (1993).

[21] J. Miyawaki, K. Yamanouchi, and S. Tsuchiya, J. Chem. Phys. **99**, 254 (1993).

[22] N. Changlong, L. Hua, and J. Pfab, J. Phys. Chem. **97**, 7458 (1993).

[23] V. P. Hradil, T. Suzuki, S. A. Hewitt, P. L. Houston, and B. J. Whitaker, J. Chem. Phys. **99**, 4455 (1993).

[24] (a) E. A. Rohlfing and J. J. Valentini, J. Chem. Phys. **83**, 521 (1985); (b) T. J. Butenhoff and E. A. Rohlfing, *ibid.* **99**, 5460 (1993); (c) **99**, 5469 (1993).

[25] H. Katagiri and S. Kato, J. Chem. Phys. **99**, 8805 (1993).

[26] A. E. Douglas and K. P. Huber, Can. J. Phys. **43**, 74 (1965); A. E. Douglas, J. Chem. Phys. **45**, 1007 (1966).

[27] L. Burnelle, A. M. May, and R. A. Gangi, J. Chem. Phys. **49**, 561 (1968); R. A. Gangi and L. Brunelle, *ibid.* **55**, 851 (1971).

[28] G. D. Gillespie and A. U. Khan, J. Chem. Phys. **65**, 1624 (1976); G. D. Gillespie, A. U. Kahn, A. C. Wahl, R. P. Hosteny, and M. Krauss, *ibid.* **63**, 3245 (1975).

[29] D. Hsu, D. L. Monts, and R. N. Zare, *Spectral Atlas of Nitrogen Dioxide 5530 to 6480 Å* (Academic, New York, 1978); P. J. Brucat and R. N. Zare, Mol. Phys. **55**, 277 (1985).

[30] H. Köppel, W. Domcke, and L. S. Cederbaum, Adv. Chem. Phys. **57**, 59 (1984); E. Haller, H. Köppel, and L. S. Cederbaum, J. Mol. Spectrosc. **111**, 377 (1985); Th. Zimmermann, H. Köppel, and L. S. Cederbaum, J. Chem. Phys. **91**, 3934 (1989); Th. Zimmermann, L. S. Cederbaum, H.-D. Meyer, and H. Köppel, J. Phys. Chem. **91**, 4446 (1987); Th. Zimmermann, L. S. Cederbaum, and H. Köppel, Ber. Bunsenges. Phys. Chem. **92**, 217 (1988).

[31] J. C. D. Brand and P. H. Chiu, J. Mol. Spectrosc. **75**, 1 (1977).

[32] K. E. Hallin and A. J. Merer, J. Mol. Spectrosc. **65**, 75 (1977); Can. J. Phys. **54**, 1157 (1976).

[33] A. Perrin, C. Camy-Peyret, and J. M. Fland, J. Mol. Spectrosc. **88**, 237 (1981).

[34] G. Persch, H. J. Vedder, and W. Demtröder, Chem. Phys. **105**, 471 (1986); J. Mol. Spectrosc. **123**, 356 (1987); H. J. Vedder, M. Schwarz, H.-J. Foth, and W. Demtröder, *ibid.* **97**, 92 (1983); G. Persch, E. Mehdizadeh, W. Demtröder, Th. Zimmermann, H. Köppel, and L. S. Cederbaum, Ber. Bunsenges. Phys. Chem. **92**, 312 (1988).

[35] H. G. Weber and F. Bylicki, Acta Phys. Pol. A **69**, 699 (1986); F. Bylicki, H. G. Weber, H. Zsheeg, and M. Arnold, J. Chem. Phys. **80**, 1791 (1984); F. Bylicki and H. G. Weber, Chem. Phys. **70**, 299 (1982).

[36] K. Uehara and H. Sasada, *High Resolution Spectral Atlas of Nitrogen Dioxide 559–597 nm* (Springer, Berlin, 1985).

[37] K. K. Lehmann and S. L. Coy, J. Chem. Phys. **83**, 3290 (1985); S. L. Coy, K. K. Lehmann, and F. C. DeLucia, *ibid.* **85**, 4297 (1986); K. K. Lehmann and S. L. Coy, Ber. Bunsenges. Phys. Chem. **92**, 306 (1988).

[38] G. Hirsch and R. J. Buenker, Can. J. Chem. **63**, 1452 (1985); G. Hirsch, R. J. Buenker, and C. Petrangolo, Mol. Phys. **70**, 835 (1990).

[39] H. Nagai, K. Shibuya, and K. Obi, J. Chem. Phys. **93**, 7656 (1990); S. Hiraoka, K. Shibuya, and K. Obi, J. Mol. Spectrosc. **126**, 427 (1987); K. Shibuya, T. Kusumoto, H. Nagai, and K. Obi, Chem. Phys. Lett. **152**, 129 (1988); S. Hiraoki, K. Shibuya, and K. Obi, J. Mol. Spectrosc. **129**, 427 (1987).

[40] K. Yamanouchi, S. Takeuchi, and S. Tsuchiya, Prog. Theor. Phys. Suppl. **98**, 420 (1989).

[41] C. F. Jackels and E. R. Davidson, J. Chem. Phys. **64**, 2908 (1976); **65**, 2941 (1976).

[42] J. L. Hardwick, J. Mol. Spectrosc. **109**, 85 (1985).

[43] R. E. Smalley, L. Wharton, and D. H. Levy, J. Chem. Phys. **63**, 4989 (1975).

[44] A. Delon and R. Jost, J. Chem. Phys. **95**, 5686 (1991); **95**, 5700 (1991).

[45] C. H. Chen, D. W. Clark, M. G. Payne, and S. D. Kramer, Opt. Commun. **32**, 391 (1980).

[46] S. J. Klippenstein, J. Chem. Phys. **96**, 367 (1992).

[47] S. I. Ionov, H. F. Davis, K. Mikhaylichenko, L. Valachovic, R. A. Beaudet, and C. Wittig, J. Chem. Phys. **101**, 4809 (1994).

[48] P. Andresen and E. W. Rothe, J. Chem. Phys. **82**, 3634 (1985).

[49] R. Schinke, V. Engel, P. Andresen, D. Häusler, and G. G. Balint-Kurti, Phys. Rev. Lett. **55**, 1180 (1985).

[50] T. Ericson, Ann. Phys. **23**, 390 (1963); Phys. Rev. Lett. **5**, 430 (1960).

[51] I. Rotter, Rep. Prog. Phys. **54**, 635 (1991).

[52] G. R. Satchler, *Introduction to Nuclear Reactions* (Oxford University, New York, 1990), pp. 252–256.

[53] R. W. Shaw, Jr., J. C. Norman, R. Vandenbosch, and C. J. Bishop, Phys. Rev. **184**, 1040 (1968).

[54] J. Main and G. Wunner, Phys. Rev. Lett. **69**, 586 (1992).

[55] R. Blümel and U. Smilansky, Phys. Rev. Lett. **60**, 477 (1988).

[56] E. T. Arawaka and A. H. Nielsen, J. Mol. Spectrosc. **2**, 413 (1958).

[57] M. D. Olman and C. D. Hause, J. Mol. Spectrosc. **26**, 241 (1968).

[58] V. Dana and J. P. Maillard, J. Mol. Spectrosc. **71**, 1 (1978).

[59] R. A. Toth and R. H. Hunt, J. Mol. Spectrosc. **79**, 182 (1980).

[60] L. Bigio and E. R. Grant, J. Phys. Chem. **89**, 5855 (1985); J. Chem. Phys. **87**, 360 (1987).
[61] K. Someda, H. Nakamura, and F. H. Mies, Prog. Theor. Phys. Suppl. (in press).
[62] M. Desouter-Lecomte and F. Culot, J. Chem. Phys. **98**, 7819 (1993).
[63] W. Iskra, I. Rotter, and F.-M. Dittes, Phys. Rev. C **47**, 1086 (1993).
[64] U. Peskin, W. H. Miller, and H. Reisler (unpublished results).
[65] R. Schinke, *Photodissociation Dynamics* (Cambridge University, Cambridge, 1993).
[66] J. L. Hardwick and J. C. D. Brand, Chem. Phys. Lett. **21**, 458 (1973).
[67] A. Weaver, R. B. Metz, S. E. Bradforth, and D. M. Neumark, J. Chem. Phys. **90**, 2070 (1989).
[68] K. Shibuya, T. Kusumoto, H. Nagai, and K. Obi, J. Chem. Phys. **95**, 720 (1991); H. Nagai, K. Aoki, T. Kusumoto, K. Shibuya, and K. Obi, J. Phys. Chem. **95**, 2718 (1991); K. Aoki, H. Nagai, K. Hoshina, and K. Shibuya, *ibid.* **97**, 8889 (1993).
[69] A. Tramer and R. Voltz, in *Excited States* (Academic, New York, 1979), Vol. 4, pp. 281–394.
[70] J. Zakrzewski, S. Saini, and H. S. Taylor, Chem. Phys. Lett. **145**, 555 (1988); J. Zakrzewski and H. S. Taylor, Phys. Rev. A **38**, 3732 (1988).
[71] R. D. Levine, Ber. Bunsenges. Phys. Chem. **92**, 222 (1988).
[72] W. H. Miller, R. Hernandez, C. B. Moore, and W. F. Polik, J. Chem. Phys. **93**, 5657 (1990); R. Hernandez, W. H. Miller, C. B. Moore, and W. F. Polik, *ibid.* **99**, 950 (1993).
[73] W. Polik, D. R. Guyer, and C. B. Moore, J. Chem. Phys. **92**, 3453 (1990).
[74] A. Delon, P. Dupre, and R. Jost, J. Chem. Phys. **99**, 9482 (1993).
[75] (a) F. H. Mies, J. Chem. Phys. **51**, 787 (1969); (b) **51**, 798 (1969); (c) Phys. Rev. **175**, 164 (1968).
[76] F. H. Mies and M. Krauss, J. Chem. Phys. **45**, 4455 (1966).
[77] M. Quack and J. Troe, in *Theoretical Chemistry: Advances and Perspectives* (Academic, New York, 1981), Vol. 6B.
[78] G. G. Hall and R. D. Levine, J. Chem. Phys. **44**, 1567 (1966); R. D. Levine, *ibid.* **44**, 2029 (1966); **44**, 2035 (1966); **44**, 2046 (1966); *Quantum Mechanics of Molecular Rate Processes* (Oxford University, Oxford, 1969).
[79] M. Bixon and J. Jortner, J. Chem. Phys. **48**, 715 (1968); M. Bixon, J. Jortner, and Y. Dothan, Mol. Phys. **17**, 109 (1969); J. Jortner and S. Mukamel, in *Molecular Energy Transfer*, edited by R. D. Levine and J. Jortner (Wiley, New York, 1974); J. Jortner and R. D. Levine, Adv. Chem. Phys. **47**, 1 (1982).
[80] W. H. Press, S. A. Teukolsky, W. T. Vettering, and B. R. Flannery, *Numerical Recipes in Fortran: The Art of Scientific Computing* (Cambridge University, Cambridge, 1992).
[81] J. Dagpunar, *Principles of Random Variate Generation* (Oxford University, Oxford, 1988).
[82] M. D. Morse and K. F. Freed, J. Chem. Phys. **74**, 4395 (1981); **78**, 6045 (1983); Chem. Phys. Lett. **74**, 49 (1980); M. D. Morse, K. F. Freed, and Y. B. Band, J. Chem. Phys. **70**, 3064 (1979); **70**, 3620 (1979); K. F. Freed and Y. B. Band, in *Excited States*, edited by E. Lim (Academic, New York, 1978), Vol. 3.
[83] J. A. Beswick and W. M. Gelbart, J. Phys. Chem. **84**, 3148 (1980).
[84] C. X. W. Qian, A. Ogai, J. Brandon, Y. Y. Bai, and H. Reisler, J. Phys. Chem. **95**, 6763 (1991).
[85] H. Grinberg, K. F. Freed, and C. J. Williams, J. Chem. Phys. **92**, 7283 (1990).
[86] R. Schinke, V. Engel, and V. Staemmler, J. Chem. Phys. **83**, 4522 (1985).